UNIVERSITY OF MINNESOTA

This is to certify that I have examined this copy of a doctoral thesis by

Rupak Mahapatra

and have found that it is complete and satisfactory in all respects,
and that any and all revisions required by the final
examining committee have been made.

Name of Faculty Adviser

Signature of Faculty Adviser

Date

GRADUATE SCHOOL

Measurements of the Mass, Total Width and Two-photon Partial Width of the Etac Meson

A THESIS
SUBMITTED TO THE FACULTY OF THE GRADUATE SCHOOL
OF THE UNIVERSITY OF MINNESOTA
BY

Rupak Mahapatra

IN PARTIAL FULFILLMENT OF THE REQUIREMENTS
FOR THE DEGREE OF
DOCTOR OF PHILOSOPHY

Professor Yuichi Kubota, Advisor

December, 2000

©Rupak Mahapatra 2000

ALL RIGHTS RESERVED

Measurements of the Mass, Total Width and Two-photon Partial Width of the Etac Meson

by Rupak Mahapatra
Under the supervision of Professor Yuichi Kubota

Abstract

Using 13.4 fb^{-1} of data collected with the CLEO detector at the Cornell Electron Storage Ring, we have observed 300 events for the two-photon production of ground state pseudo-scalar charmonium η_c decaying into $K^0_S K^{\mp}\pi^{\pm}$. We have measured the mass and total width of η_c to be (2980.4 $\pm$ 2.3 (stat) $\pm$ 0.6 (syst)) MeV and (27.0 $\pm$ 5.8 (stat) $\pm$ 1.6 (syst)) MeV, respectively. From the production rate, we have also extracted the two-photon partial width of η_c to be (7.6 $\pm$ 0.8 (stat) $\pm$ 0.4 (syst) $\pm$ 2.3 (br. syst)) keV, with the last uncertainty associated with the decay branching fraction. Our results imply a value of the strong coupling constant α_s at the charm scale to be 0.285 $\pm$ 0.025.

Acknowledgments

Life has given me this wonderful opportunity to learn the beauty of Physics in many different ways since my childhood and I am deeply indebted to everyone who has taught me Physics and given me an opportunity to be involved in the quest to understand the deepest and the most beautiful wonders of the universe. My father has always been a role model for me since my childhood, teaching me science by example. I had the fortune of being guided by the right people at the right time which helped me in materializing my dream of taking up Physics as my life long career.

During my high-school Rajni K. Mohanty initiated me into learning more about Physics. The turning point of my life came during my undergraduate degree in Chemical Engineering, when G. P. Sastry at the Indian Institute of Technology taught me the beauties of Physics in general and Quantum Mechanics and Particle Physics in particular. Then, at the University of Minnesota, I had the fortune of being guided by Ron Poling and Yuichi Kubota, when I was lost at a crucial juncture of my career. Ron has been a wonderful fatherly figure, always there to count upon and giving the right advice. Yuichi has been an wonderful teacher, who has always insisted that things be done right, no matter how hard they might seem at the beginning. Yuichi also has been a good friend who has listened to and shared his concerns in any worries of my life. The most cherished memory of my graduate education will be what Yuichi has helped me become, to be an independent minded researcher who strives hard to achieve the set goal. I had the good fortune of having all the freedom of thoughts and deeds, in both the Physics analyses and the hardware works.

I owe it most to my father who has been the most important motivating factor in my education in science in general and Physics in particular, with always the encouragement to be the best in whatever I do and to be honest. I am also indebted to my mother for all her love, my brother for his friendship and support at crucial junctures in my life. I am thankful to my wife for her love, encouragement and prayers for my success.

I am especially thankful to Rich Galik who guided me and provided me all sorts of help during my stay at Cornell. I am deeply indebted to Vladimir Savinov who mentored me during my initial days at CLEO and helped me learn the details of two-photon physics. I am also thankful to my fellow Minnesota CLEOns Sang-Joon Lee, Stefan Anderson, Alex Smith and Tim Riehle for their friendship and help. I am grateful to the CLEO and CESR staff for facilitating this thesis research.

Contents

List of Figures

List of Tables

1. INTRODUCTION

This thesis describes measurements of the mass, total decay width and two-photon partial width of the ground state pseudo-scalar charmonium ($c\bar{c}$ bound state) η_c ($J^{PC} = 0^{-+}$) produced in two-photon fusion process of the following kind:

$$e^+e^- \to e^+e^-\gamma\gamma \to e^+e^-\eta_c. \tag{1}$$

A by-product of e^+e^- collision experiments is that each lepton can emit a virtual space-like photon which can interact with each other. This is known as the two-photon Physics and stands for the process $e^+e^- \to e^+e^-R$, where R is any of the C-even (since photon has odd C-parity) final states. Though the cross-section for this two-photon process is down by two powers of α ($= e^2/4\pi = 1/137$) compared to the dominant annihilation process, the radiation of a photon leads to a double bremsstrahlung factor of $\ln^2(s/m_e^2)$, which at sufficiently high energies can more than compensate.

Production of these even C-parity hadronic matter in e^+e^- scattering provides an unique opportunity to study the properties of strong interactions. This analysis is focussed on the two-photon production of the ground state pseudo-scalar charmonium ($c\bar{c}$ bound state) η_c. The charmonium spectrum is ideal for testing quantum chromodynamics (QCD) calculations. Furthermore, producing the C-even charmonium through two-photon fusion process provides a very clean environment for this purpose, since the initial states in the e^+e^- scattering are very well understood, and an interpretation of the production of the hadron can focus only on understanding the final state.

The quarkonium (quark-antiquark pair) system is similar to the positronium system (e^+e^- bound state). In the same way that the positronium is used to study quantum electrodynamics (QED), quarkonium can be used to test the validity of various QCD calculations and assumptions we make in the calculations. The advantage of studying heavy quarkonium lies in the fact that the quarks are non-relativistic. Non-Abelian SU(3) theory predicts asymptotic freedom[1] for the quarks at short distances, *i. e.* the coupling between the quarks is small at short distances. In low lying heavy quarkonia the characteristic distance is much smaller than the QCD scale. Therefore, multiple gluon exchange between the two quarks is small. Hence, in the language of QCD, the short-distance interaction between the two quarks is dominated by single-gluon exchange, just as it is dominated by single-photon exchange in QED.

Since the gluon and the photon are both massless spin-1 particles, the interactions are approximately similar up to the overall coupling constants (α in QED and α_s in QCD). To study quarkonium spectra, defining a non-relativistic potential between the two quarks is useful. We know from the phenomenon of quark-confinement (we do not see free quarks) that the force between two quarks increases with the separation between them, when the separation is large. So, an *ansatz* potential having two terms - one term for the short-distance interaction between the two quarks that is inverse in r (similar to the Coulomb potential) and the other for the long distance string-like tension (confining potential) force between the two quarks that is linear in r - may be a good approximation to deduce the bound states of quarkonium systems [2],

$$V(r) = -\frac{4}{3}\frac{\alpha_s}{r} + kr. \tag{2}$$

This form of the potential works reasonably well in predicting the masses of various bound states of heavy quarks, using the masses of the ψ, ψ', and ψ'' mesons as experimental inputs to determine the coefficient of the linear confining potential term. The hyperfine splitting due to the spin-spin interaction between the two quarks can also be incorporated to predict the mass splitting between the J/ψ and the η_c charmonia. Predictions for the mass of the η_c meson have been made to be around (2978 $\pm$ 10) MeV [3]. The world average value (PDG[1]) [4] of various experimental measurements of the mass of η_c is (2979.8 $\pm$ 2.1) MeV.

When it comes to the production and decay of the quarkonium system, it becomes a theoretically much more challenging task to predict various parameters, like the total width, individual branching fractions to various decay modes, etc. Production and decay of quarkonium states (any bound quark states in general) involves a long-distance confining mechanism which can only be calculated non-perturbatively and a short-distance interaction among the quarks which have been relatively well understood using formulations of perturbative QCD (PQCD). It is hard to do non-perturbative calculations of QCD. Lattice QCD calculations of non-perturbative processes are still in their infancy. In addition, the interplay between these perturbative and non-perturbative aspects of the bound state dynamics is often non-trivial and analytically in-separable. However, at short distances, the perturbative QCD treatment predicts the production and decay parameters of heavy quarkonium reliably.

---

[1]From now onwards, we refer to Ref. 4 as PDG

The ratios of two decay rates are calculated with a small theoretical error since the non-perturbative components cancel out. Inclusive decays are especially amenable to PQCD treatment, although predictions for some exclusive decays have also been made [5]. Theoretical predictions have been made possible using perturbative QCD for a large number of experimentally accessible phenomena [2].

Two of the most important parameters that are calculable from perturbative QCD are the total width and two-photon partial widths of the charmonium η_c (relative to other well measured quantities), and their experimental measurements provide important verification for the validity of the calculations and various approximations. Calculations only up to the next-to-leading order (NLO) in α_s have been done so far. Next-to-next-leading order (NNLO) calculations, though difficult, may be necessary, if experimental results disagree strongly with the theoretical calculations.

The two-photon partial width $\Gamma^{\eta_c}_{\gamma\gamma}$ can be expressed in NLO in terms of the e^+e^- width of J/ψ as follows [6]

$$\frac{\Gamma(\eta_c \to \gamma\gamma)}{\Gamma(\psi \to e^+e^-)} = \frac{4}{3}(1 + 1.96\frac{\alpha_s}{\pi})\frac{M_\psi^2}{(2m_c)^2}\frac{|\Psi_{\eta_c}(0)|^2}{|\Psi_\psi(0)|^2}. \tag{3}$$

Assuming the wave function at the origin $|\Psi(0)|^2$ is the same for the two 1S states (only spin is different), and setting $2m_c \approx M_\psi$, one gets

$$\frac{\Gamma(\eta_c \to \gamma\gamma)}{\Gamma(\psi \to e^+e^-)} = \frac{4}{3}(1 + 1.96\frac{\alpha_s}{\pi}) \approx 1.6, \tag{4}$$

where the value of α_s evaluated at charm scale has been used $\approx (0.28 \pm 0.02)$[6]. This, combined with the experimental average value of $\Gamma^{\psi}_{e^+e^-} \approx (5.3 \pm 0.4)$ keV [4], gives an estimate of $\Gamma^{\eta_c}_{\gamma\gamma} \approx (8.2 \pm 0.6)$ keV. Relativistic corrections to the above calculation brings the prediction down the to 6-7 keV [7]. The PDG average of various experimental measurements of $\Gamma^{\eta_c}_{\gamma\gamma}$ is (7.5 ± 1.5) keV.

One should note that the assumption of the two 1S wave functions being the same at the origin to estimate $\Gamma^{\eta_c}_{\gamma\gamma}$ may have large uncertainties, where the effects of hyperfine interactions affecting the wave functions have been ignored. The magnetic transition $J/\psi \to \gamma\eta_c$ was observed to be [8] about three times weaker than one estimates non-relativistically [9]. This disagreement may be an indication that the effect of hyperfine interaction on the η_c and J/ψ wave functions is non-trivial. A detailed discussion on these issues may be found in Appendix D.

The total width of η_c can be assumed to be dominated by the two-gluon decay,

$$\Gamma_{tot}(\eta_c) \approx \Gamma(\eta_c \to gg). \tag{5}$$

Because, the ratio of the rates of the two annihilation process of the η_c to 2 gluons and 2 photons depends only on the coupling constants, one can obtain the following relationship [6],

$$\frac{\Gamma(\eta_c \to gg)}{\Gamma(\eta_c \to \gamma\gamma)} = \frac{9\alpha_s^2}{8\alpha^2}\frac{(1+4.8\alpha_s/\pi)}{(1-3.4\alpha_s/\pi)}, \tag{6}$$

where the simple (lowest order in α_s) ratio of $9\alpha_s^2/8\alpha^2$ has been multiplied by the NLO QCD correction factor for $\eta_c \to gg$ of $(1+4.8\alpha_s/\pi)$ and NLO QCD correction factor for $\eta_c \to \gamma\gamma$ of $(1-3.4\alpha_s/\pi)$. The ratio of these two widths is an especially clean prediction of perturbative QCD, since the dependence on wave functions and $O(v^2/c^2)$ non-perturbative corrections cancel out [10]. The above predicted ratio is 3400 ± 700.

Using the value of $\alpha_s \approx (0.28 \pm 0.02)$ and the previous estimation $\Gamma_{\gamma\gamma}^{\eta_c}$ of (8.2 ± 0.6) keV, one obtains an estimate of $\Gamma_{tot}^{\eta_c}$ as (28 ± 6) MeV. On the other hand, using the PDG average of $\Gamma_{\gamma\gamma}^{\eta_c}$ as (7.5 ± 1.5) keV, one obtains an estimate of $\Gamma_{tot}^{\eta_c}$ as (26 ± 6) MeV. Calculation done with fully relativistic decay amplitudes and a sophisticated QCD potential model [11] predict $\Gamma_{\rm tot}^{\eta_c} \approx 23$ MeV, using the experimental value of $\Gamma_{\gamma\gamma}^{\eta_c}$ as an input. The current world average, $\Gamma_{tot}^{\eta_c} = 13.2^{+3.8}_{-3.2}$ MeV [4] disagrees with these theoretical expectations. The individual measurements contributing to the above average have large individual uncertainties and differ from each other significantly.

Hence, a precise measurement of the total width and two-photon partial width of the η_c meson is very important for the verification of these calculations, especially with the present clear disagreement between the theoretically predicted total width of the η_c and the experimental average.

2. THEORY OF MESON PRODUCTION IN TWO-PHOTON PROCESS

The process of interest is the production of a C-even meson from two space-like photons, each emitted from the e^+ and e^- beams,

$$e^+e^- \to e^+e^-\gamma\gamma \to e^+e^-R, \tag{7}$$

where R is the η_c meson.

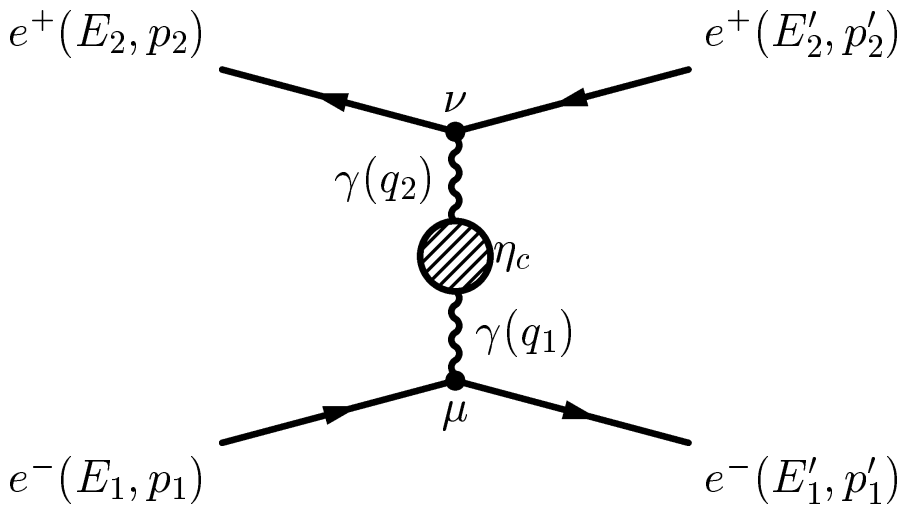

Fig. 1. Two-photon production of η_c.

The complete quantum mechanical description of the two-photon production of a resonance, as shown in Figure 1, has the amplitude [12]

$$M = -e^2 \bar{u}(p_1')\gamma^\mu u(p_1) v(p_2)\gamma^\nu \bar{v}(p_2') \frac{1}{q_1^2 q_2^2} T_{\mu\nu}. \tag{8}$$

The term $T_{\mu\nu}$, describing the hadron production from the two virtual photons, contains the physics of interest. It is therefore useful to disentangle the leptonic part, which is completely calculable from QED, from the $\gamma\gamma \to$ hadrons vertex. The result has been given by V. M. Budnev *et al* [13] and others. For unpolarized electron beams,

$$d\sigma = \frac{\alpha^2}{16\pi^4 q_1^2 q_2^2} \sqrt{\frac{(q_1 q_2)^2 - q_1^2 q_2^2}{(p_1 p_2)^2 - m_1^2 m_2^2}} \{4\rho_1^{++}\rho_2^{++}\sigma_{TT} + 2|\rho_1^{+-}\rho_2^{+-}|\tau_{TT}\cos(2\phi)$$

$$+2\rho_1^{++}\rho_2^{00}\sigma_{TL} + 2\rho_1^{00}\rho_2^{++}\sigma_{LT} + \rho_1^{00}\rho_2^{00}\sigma_{LL} - 8|\rho_1^{+0}\rho_2^{+0}|\tau_{TL}\cos(\phi)\} \frac{d^3p_1'}{E_1'} \frac{d^3p_2'}{E_2'}, \tag{9}$$

where, ρ^{ab} are the photon flux factors and labels $+$, $-$, 0 refer to the helicities of the photons in the $\gamma\gamma$ center of mass system. The angle ϕ is the angle between the electron-γ planes in the $\gamma\gamma$ center of mass system. The suffixes T and L for the cross section terms σ and τ stand for combinations of transverse and longitudinal photon contribution to the total cross section; so σ_{TT} corresponds to the cross-section

term for a transverse photon interacting with a transverse photon. The τ terms represent the cross terms. For example, τ_{TT} represents the difference between cross-sections for scattering transverse photons with the parallel ($\sigma_{\parallel}$) and orthogonal ($\sigma_{\perp}$) linear polarizations. So, $\tau_{TT} = \sigma_{\parallel}$ - $\sigma_{\perp}$, whereas $\sigma_{TT} = (\sigma_{\parallel} + \sigma_{\perp})/2$. For detailed descriptions of each of the terms in the above cross-section equation and a better understanding of two-photon fusion mechanism, one should refer to Appendix A, which contains summary extracted from Reference [12] [13].

The coupling of a neutral pseudo-scalar meson to two photons proceeds through a single amplitude and hence, there is only one form factor $F(q_1^2, q_2^2)$

$$T_{\mu\nu} = i\epsilon_{\mu\nu\alpha\beta} q_1^{\alpha} q_2^{\beta} F(q_1^2, q_2^2). \tag{10}$$

A direct consequnce of the form of the amplitude is that a 0^- state cannot couple to longitudinally polarized photons. The only nonzero terms entering the full $e^+e^- \to e^+e^-R$ formula are

$$\sigma_{TT} = -\frac{1}{2}\tau_{TT} = \frac{\sigma_{\perp}}{2} = \frac{1}{4}F^2(q_1^2, q_2^2)\frac{M_R^2\sqrt{(q_1q_2)^2 - q_1^2q_2^2}}{W_{\gamma\gamma}}\frac{\Gamma}{(W_{\gamma\gamma}^2 - M_R^2)^2 + \Gamma^2 M_R^2}, \tag{11}$$

where Γ is the total width of the resonance, M_R is the pole mass of the meson and $W_{\gamma\gamma}$ is the invariant mass of the two photons.

The form factor at the origin is related to the two-photon partial width as

$$F^2(0,0) = \frac{64\pi\Gamma_{\gamma\gamma}}{M_R^3}. \tag{12}$$

A simple vector meson dominance model (VDM) prediction for the q_1^2 and q_2^2 dependence of the form factor is [12]

$$F_{\eta_c\gamma\gamma}(q_1^2, q_2^2) = \frac{F(0,0)}{(1 - \frac{q_1^2}{m_{\psi}^2})(1 - \frac{q_2^2}{m_{\psi}^2})}, \tag{13}$$

where the form factor factorizes into two terms as $F(q_1^2, q_2^2) = F(q_1^2) \cdot F(q_2^2)$.

The transition form factor $F(q_1^2, q_2^2)$ can not be calculated directly from QCD. However, it has been estimated using perturbative QCD, sum-rules approach, and other theoretical methods. Perturbative QCD calculation for the $\eta_c\gamma\gamma$ form factor, where one of the photons is off-shell, gives the form of a single pole form factor with the pole mass dominated by the J/ψ mass [2],

$$F_{\eta_c\gamma\gamma}(q_1^2, q_2^2 = 0) = \frac{64\pi}{M_R^3}\frac{\Gamma_{\gamma\gamma}}{(1 - \frac{q^2}{m_{\psi}^2})}, \tag{14}$$

for $Q^2(=-q^2) < M_{\eta_c}^2$. The corrections to the J/ψ dominance are found to be $\leq O(\alpha_s(m_c))$. This agrees with the VDM prediction also [12].

However, when both the photons are off-shell, this prediction differs substantially from the VDM prediction of a double pole form factor, and predicts the form factor $\eta_c\gamma\gamma$ as [14]

$$F_{\eta_c\gamma\gamma}(q_1^2, q_2^2) = \frac{F(0,0)}{(1 - \frac{q_1^2}{m_\psi^2} - \frac{q_2^2}{m_\psi^2})}. \tag{15}$$

This uncertainty in the form factor does not lead to any marked difference in the cross-section for low values of q^2 ($\rightarrow 0$).

In the two photon cross section, the amplitude due to the photon propagators naturally peak at $q^2 \rightarrow 0$, majority of events involve almost-real photons and the produced resonance has low transverse momentum. The scattered leptons remain close to the incident direction and are not generally detected. Two photon events can be classified by the number of the scattered leptons which are detected. Where neither is detected, one has 0-tag (untagged) events, which form the major part of two-photon data. We search for two-photon production of the η_c meson in this untagged mode.

3. THE DETECTOR

The CLEO detector is a general-purpose magnetic spectrometer. It was operated at the Cornell Electron Storage Ring (CESR) which is a symmetric e^+e^- collider running at the center-of-mass energy around 10.6 GeV. The CLEO detector was used in two configurations - CLEO II[15] from 1990 to 1995 and CLEO II.V[16] from 1995 to 1998. The straw-tube vertex detector in CLEO II was replaced by a high resolution silicon vertex detector in CLEO II.V.

The CLEO detector provided energy, momentum and direction measurements of the particles that passed through its active components when beams of electrons and positrons collided in the interaction region which was situated in the geometrical center of the detector. The active components of the CLEO detector included central tracking detectors, time-of-flight scintillator (TOF) counters, an electromagnetic calorimeter and muon detectors. All systems except the muon detectors resided inside an uniform solenoidal magnetic field of 1.5 Tesla.

The central tracking detectors covered 95% of the solid angle and consisted of three concentric cylindrical detectors. From smallest to largest radii these were: the

precision tracking layer (PTL) detector, the vertex detector (VD) and the main drift chamber (DR) for the CLEO II configuration. For the CLEO II.V configuration, the PTL detector was replaced with a silicon vertex detector (SVX).

The PTL detector consisted of tubular drift cells that were arranged in six concentric layers of 64 cells. The spatial resolution of PTL depended on the gas used. It was about 110 μm for 50:50 Argon-Ethane gas and about 55 μm for Dimethyl Ether (DME). This chamber was employed to improve momentum resolutions and localization of primary and secondary vertices.

The SVX detector consisted of 3 layers of double-sided silicon wafers placed at radii 2.35 cm, 3.25 cm and 4.75 cm, respectively. A total of three layers were chosen to provide high efficiency for measurement of at least two hits. Positioning the silicon wafers so close to the beam pipe allowed the measurement of the z-coordinate of a particle trajectory (coordinate along the beam axis), prior to the degradation of that coordinate caused by multiple Coulomb scattering in the inner detector material. Each silicon wafer had implants on both sides, with n-type implants facing the beam axis, and arranged perpendicular to the beam axis, to measure the z-coordinate of a particle trajectory. On the opposite side, away from the beam axis, p-type implants parallel to the beam measured the ϕ coordinate. The detector was comprised of 96 silicon wafers containing 26208 channels and covered 92% of the solid angle. The cross-sectional $r\phi$ and rz views can be seen in Figure 2. The spatial resolution depended on the entrance angle of the track and was about 30 μm at normal incidence, which was a significant improvement over the PTL detector. The CLEO II.V SVX detector was designed primarily to resolve D-meson and τ-lepton decay vertices. For our analysis, it did not play a directly crucial role in terms of the track's positional information near the interaction point. It however gave rise to better measurements of track momenta resulting from better hit resolution.

The VD chamber contained ten cylindrical layers of sense wires and azimuthal cathode-strip segments on the inner and outer walls. The inner five layers of VD contained 64 cells each while the outer five layers of VD had 96 cells each. Both cathode layers were segmented into conducting segments both in azimuthal (ϕ) and axial (z) directions to provide precise z–position measurements and easier r-ϕ matching for the track reconstruction purposes. The electric pulses produced on a sense wire by a particle-induced avalanche were measured at both ends of the wire. The relative sizes of these electric pulses was used to obtain information about the z–position of tracks.

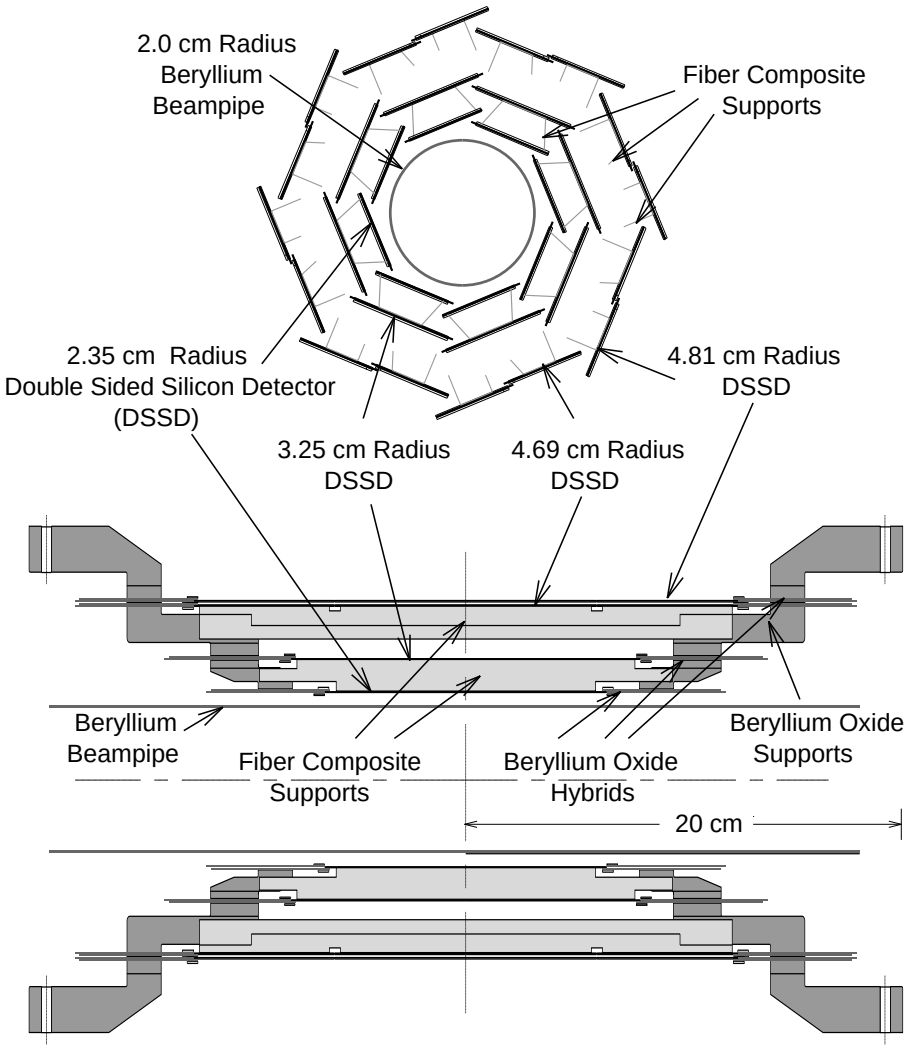

Fig. 2. CLEO II.V SVX cross-sectional $r\phi$ (top) and rz view (bottom). The $r\phi$ layout was octagonal with overlap in the corners, to provide efficiency and the ability to align the detector. In the rz projection, pairs of wafers met with no overlap at the detector center, and are read out at either end.

The spatial resolution of each cathode layer was 1.2 mm. The r-ϕ r.m.s. resolution for the VD was approximately 100 μm. The VD covered 91% of the solid angle.

The main drift chamber, DR, provided measurements of charged particles' momentum vectors and specific ionization energy losses (dE/dx). This chamber consisted of 51 layers of rectangular cells and inner and outer cylindrical cathodes. There were two types of wire layers, axial and stereo. Stereo cells contained wires that were slightly slanted with respect to axial wires. The spatial resolutions of axial and stereo cells were 190μm and 230μm, respectively. Stereo cells as well as inner and outer cathodes provided z–position measurements. The spatial resolution of the DR cathode was 1.8 mm.

The pulse heights measured in DR provided dE/dx measurements that are employed in particle identification. Since the energy loss depends on the velocity of an ionizing particle, the expected pulse height for a particle of given momentum would be different depending on the particle mass. The dE/dx provided separation of π and K up to 0.8 GeV/c. The ionization energy losses per unit path length are shown in Figure 3 for particles of various species.

The gas in the tracking devices was changed from 50:50 Argone-Ethane in the CLEO II configuration to 60:40 Helium-Propane in the CLEO II.V configuration, giving rise to better tracking (due to less multiple scattering) and better dE/dx resolution.

The information from all three tracking chambers was used to reconstruct trajectories of charged particles. The transverse momentum and azimuthal angle were reconstructed from the position measurements from axial wires; polar angle was obtained from stereo wires, four cathodes and VD wires. These together achieved a relative momentum resolution

$$\frac{\sigma_p}{p}(\%) = \sqrt{(0.15p)^2 + (0.50)^2} \quad (p \text{ in GeV/c}). \tag{16}$$

The azimuthal and polar angular resolutions were $\delta\phi \approx 1$ mrad and $\delta\theta \approx 4$ mrad at normal incidence for the CLEO II configuration. With the improved resolution due to the SVX, for the CLEO II.V configuration, these values were $\delta\phi \approx 1$ mrad and $\delta\theta \approx 1$ mrad at normal incidence.

The 64 TOF counters that surrounded the main drift chamber were made of plastic scintillators and covered 96% of the solid angle. These detectors measured the time interval between the beam collision and particle's arrival at the TOF detector. The geometrical acceptance of the TOF counters were only limited by the leakage between

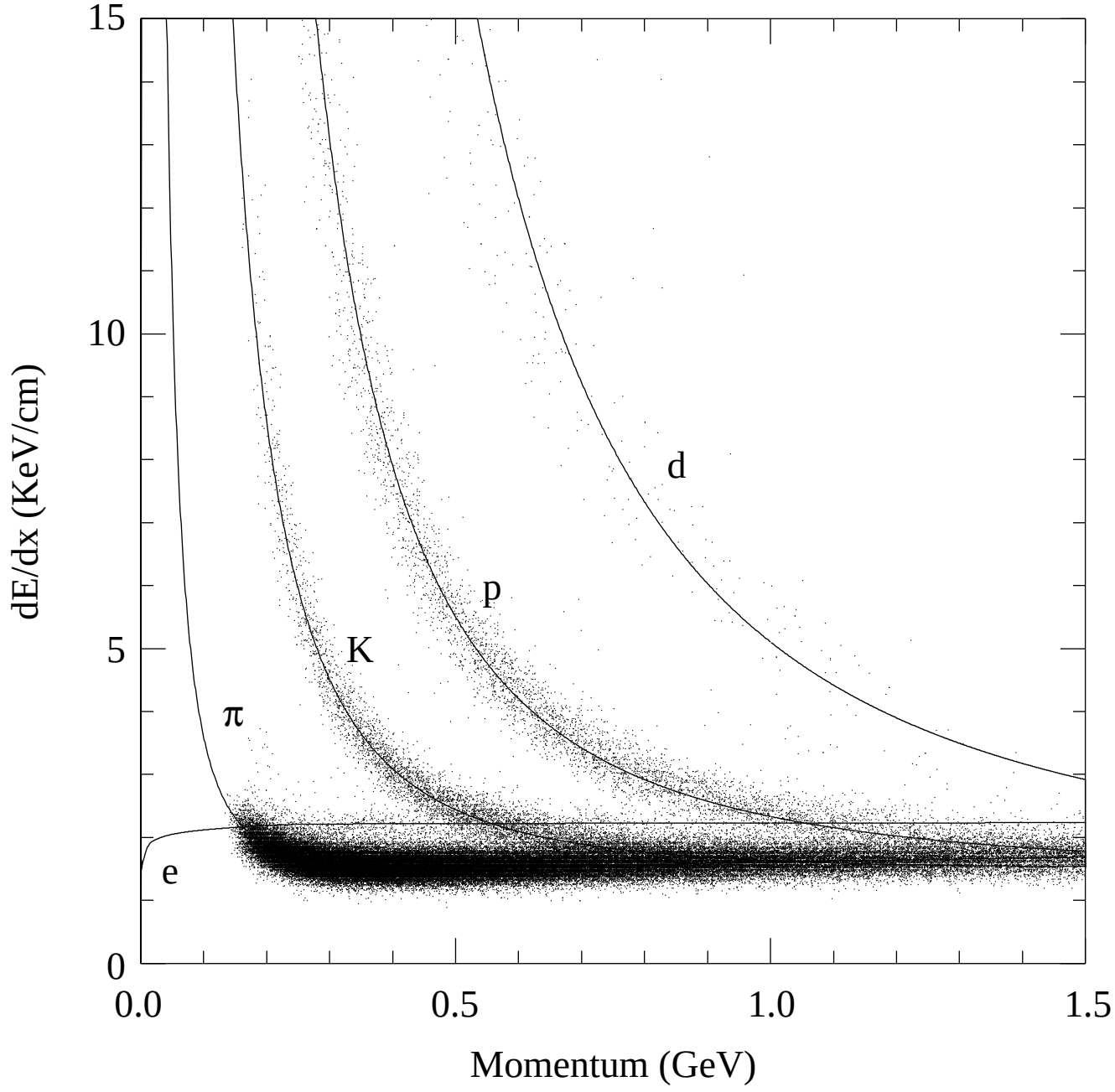

Fig. 3. The dE/dx distribution.

the scintillators. The geometrical acceptance of the barrel TOF counters was 97%. Each end of CLEO II was covered by 28 wedge-shaped endcap TOF counters with geometrical acceptance of 99.5%. These detectors were located behind the DR end plates. The TOF system was an important component of the trigger system, especially of its fast, "zeroth" level (L0). In addition, TOF counters could be used for particle identification. When the trajectory of a charged particle was reconstructed, we knew the path length this particle had traveled. By combining the path length with the time measurement from TOF, we could calculate the velocity, β, of the particle. At momenta below 1.0 GeV/c it allowed separation of charged pions and kaons. The $1/\beta$ separation for particles of different species is illustrated in Figure 4.

The electromagnetic calorimeter (CC) consisted of 7800 thallium-doped CsI scintillation crystals that covered 96% of the solid angle. There were 6144 barrel crystals, 30 cm in length (16 radiation length) and approximately 5×5 cm^2 in cross section at the front. They were oriented in such a way that their lengths were pointing to the primary interaction region. Each endcap part of the calorimeter consisted of 828 crystals stacked with their axes parallel to the beam axis. The electromagnetic calorimeter was used for photon detection.

The muon detectors were constructed using proportional counters that were embedded in the iron yoke of the super-conducting solenoid magnet of the CLEO II detector. To reach the most outer layer of the muon detectors, a charged particle needed to penetrate an amount of material equivalent to 7 nuclear absorption lengths. Only muons were able to go that far and be detected.

Side and end views of the CLEO II.V detector (for CLEO II, SVX replaced with PTL) are shown in Figures 5 and 6, respectively.

The CESR beams collide every 350 ns, but most of the collisions produce no interesting reaction. To reject unwanted events before their detector information is read out, and write to tape only those events which might be interesting for further analysis, CLEO uses 3 levels of hardware triggers (L0, L1 and L2) and one level of software selection or trigger (L3). There are many trigger conditions (trigger lines) and any event must satisfy at least one of them. Each trigger line is optimized for different physics processes. If an event passed through any L0 trigger line, then all L1 trigger lines were evaluated. If an event passed any of the L1 lines, then it was required that the corresponding L2 line also be satisfied for the event to be digitized and read out from the detector for further analysis. An event could satisfy multiple

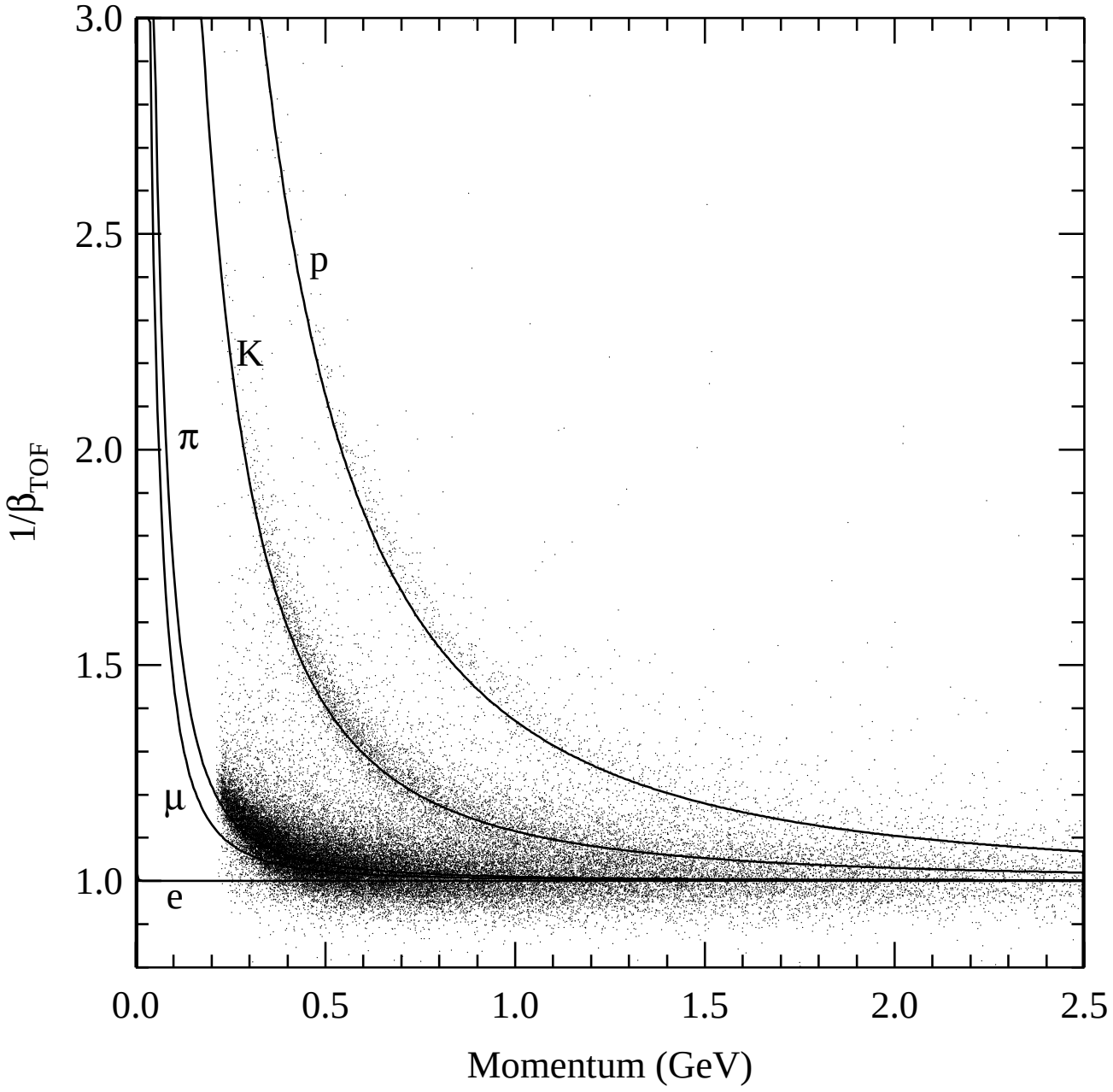

Fig. 4. The Time-of-Flight $1/\beta$ distribution.

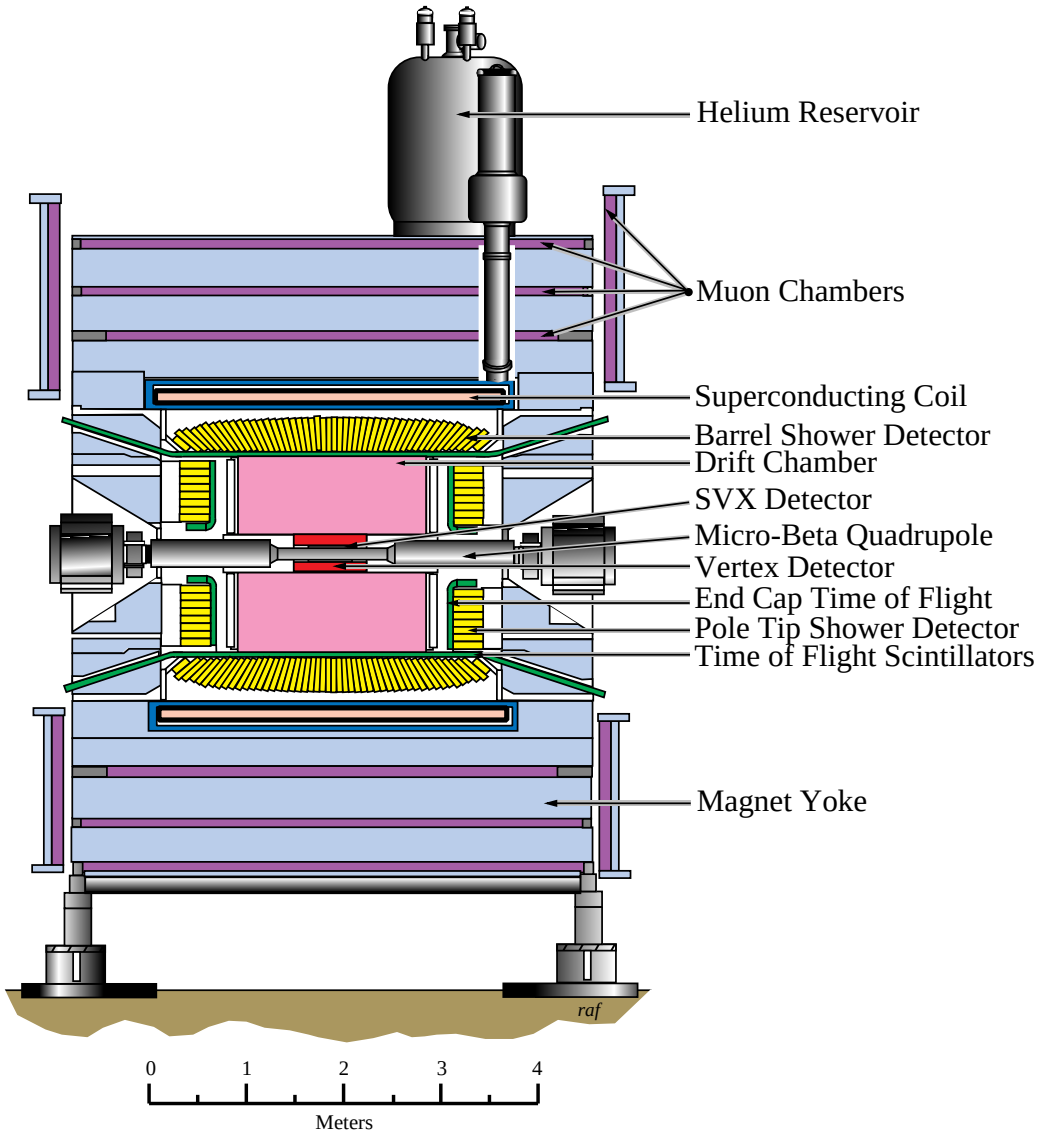

Fig. 5. The CLEO II.V detector side view.

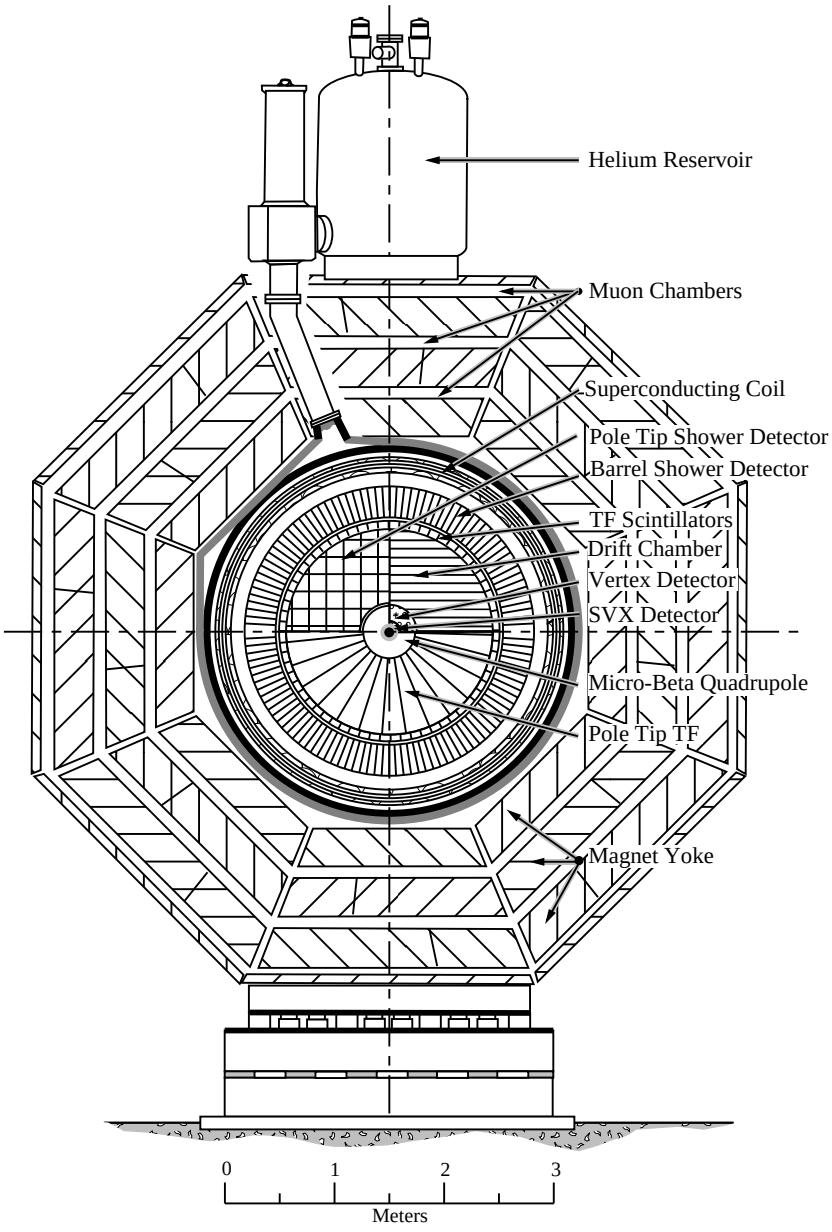

Fig. 6. The CLEO II.V detector end view sliced at three depths.

L1/L2 combinations.

The fastest, "zeroth"-level (L0) trigger used either VD and TOF or CC. For the L0 trigger purposes VD was divided into the inner and outer five layers. The VD chamber provided a L0 trigger when at least three out of each set of the five layers contained hits within one of the azimuthal sections of $\delta\phi \approx 15^\circ$ as determined by the hardware pattern recognition processor. The endcap TOF generated a L0 trigger when one of the TOF scintillators produced a pulse. The barrel TOF provided a L0 trigger when signals were detected at both ends of any barrel TOF counter. The calorimeter also provided a L0 trigger when TOF and VD triggers failed. The calorimeter generated a L0 trigger when energy cluster of about 500 MeV or more was detected. However, since the signal in the CsI crystals developed slowly, the VD and TOF trigger information had been lost by the time the calorimeter L0 trigger decision was made.

The first-level (L1) trigger utilized the information from the TOF, main drift chamber (DR) and the calorimeter (CC). The TOF components of the L0 and L1 triggers were identical. The information from the drift chambers was processed by hardware fast track reconstruction processors, Track Segment Processor (TSP) and Binary Linear Tracker (BLT).

The TSP processor used all layers of VD and twelve layers of DR to search for straight hit patterns recognized as tracks with transverse momenta above 400 MeV. The BLT processor attempted to link together the DR hits to form curved tracks originating from the primary interaction point. The BLT processor was able to identify the charge and crude transverse momentum of track by its bending radius in the magnetic field. This processor could be used to detect charged tracks with transverse momentum above 340 MeV. The calorimeter generated a L1 trigger by means of low and high threshold discriminators. The low threshold discriminator was satisfied when an energy cluster of about 100 MeV or more was found. The high threshold was achieved when energy of the cluster was above 500 MeV. For trigger purposes the calorimeter was divided into segments of 16 crystals.

The second-level (L2) trigger used BLT. Also, the earlier data sets in CLEO II had been recorded with a trigger configuration that included Precision Tracking Device (PD). The PD processor had searched for patterns of hits in VD that were consistent with charged tracks produced by particles with transverse momenta above 125 MeV. For more recent data, the L0 VD information was used in L2 trigger decisions.

The third-level trigger (L3) was a software trigger that was optimized to suppress beam-related background processes, such as electroproduction on residual gas molecules and beam-wall interactions. To be recorded, events had to pass the L3 trigger. The L3 trigger tagged and kept every 8th event it would reject in data for measuring the L3 trigger efficiency and also for verification purposes.

4. ANALYSIS

In this analysis, production of the η_c meson in two-photon process was searched for by detecting the final state particles the η_c decayed into. We studied the η_c production in the decay mode $\eta_c \to K^0_S K^\pm \pi^\mp$, where the K^0_S subsequently decayed into $\pi^+\pi^-$. In untagged two-photon production, due to the low momentum transfer to the photons, the e^+ and e^- have little transverse momentum relative to their initial direction. Hence the event has low net transverse momentum and the e^+ and e^- travel down the beam pipe un-detected. The final state has only the 4 charged tracks that the η_c decays into. In addition, since the e^- and e^+ are undetected, the event has low detected energy. There are no neutrals in the final state, hence the total energy deposited in the electromagnetic calorimeter not matched to the four charged tracks is also very low.

4.1. Data Sample

The data used in this analysis corresponded to an integrated luminosity of 13.4 fb^{-1} - 4.7 fb^{-1} in the CLEO II configuration and 8.6 fb^{-1} in the CLEO II.V configuration [17].

4.2. Monte Carlo

The $\gamma\gamma \to \eta_c \to K^0_S K^\pm \pi^\mp$ Monte Carlo was generated with a technique described in Appendix C assuming that the η_c decays into the $K^0_S K^\pm \pi^\mp$ final state via a flat 3-body phase space decay. On the other hand, there have been speculations [12] that η_c also decays via a 2-body decay into $K^*\bar{K}$, where the K^* subsequently decays into a $K^0_S\pi^\pm$ or $K^\pm\pi^\mp$, giving rise to the same $K^0_S K^\pm \pi^\mp$ final state. This decay mode would obviously have a different kinematics than the flat 3-body decay assumed in our Monte Carlo, possibly giving rise to a different detection efficiency, and hence a different two-photon partial width (if mixed with our events). As described in the resonance sub-structure systematics section, we estimated the presence and effect of this possible resonant sub-structure in the η_c decay.

The different data sets used for this analysis had different trigger conditions and hence different detection efficiencies. To take this into account, Monte Carlo genera-

tion was distributed over all the data sets with the number of events in each data set approximately scaling with the data luminosity of the corresponding data set. This method of generating Monte Carlo spread over many run numbers in many data sets not only mimicked data for similar trigger efficiency, but also took into account the variation of detector resolution from data set to data set or run-period to run-period. This way we tried to mimic the data as well as we could in the Monte Carlo. We generated Monte Carlo sample which was about 50 times the data size.

4.3. Event Selection

Events having four charged tracks with no net charge were accepted for further analysis. The track reconstruction program used in CLEO tried to reconstruct as many tracks as possible and erred on the side of reconstructing non-existing tracks from a random group of hits in the tracking chambers. This sometimes led to identification of more tracks than there actually were. For events having more than four charged tracks, a track classification package (TRKMAN) was used which identified very low momentum tracks which curled around inside the tracking volume and showed up as multiple tracks as well as tracks reconstructed from residual hits on genuine tracks. Eliminating such fake tracks gave us about 20% more events in which there were exactly four charged tracks with no net charge. Events were also required to have an identified K^0_S. Using to advantage the large K^0_S decay length ($c\tau$=2.68cm), K^0_S vertex was required to have a flight significance (ratio of flight distance to the uncertainty in the flight distance measurement) of at least 3 in CLEO II and 5 in CLEO II.V, to reduce background from K^0_S's reconstructed out of random $\pi^+\pi^-$ coming from the interaction point. A maximum chi-square cut (< 10) on the geometrical intersection of the two daughter tracks in the r-ϕ and r-z plane was applied for the K^0_S vertex fit to remove fake K^0_S's. The K^0_S candidate was accepted if its invariant mass fell within 12 MeV of the nominal K^0_S mass (497.672 MeV). Then the K^0_S candidate was required to come from the interaction point by applying a maximum chi-square cut (< 30) on the K^0_S flight direction extrapolating back to the interaction point. If there were more than 1 K^0_S candidate satisfying our K^0_S selection criteria then the event was rejected. The remaining two tracks were identified as a kaon and a pion using dE/dx and TOF information.

Two-photon events tend to have small net transverse momentum due to the peak-

ing of the cross-section at small momentum transfer to the two-photon system. To reject non-two-photon events, the net transverse momentum (P_T) of the η_c candidate was required to be less than 0.6 GeV. The total energy deposit in the calorimeter not matched to the charged tracks was required to be less than 0.6 GeV since there was no expected neutral particle in the decay of the η_c. This requirement on the unmatched neutral was kept loose to take into account the possibility of higher energy deposit in the electromagnetic calorimeter than expected, due to showers from hadronic split-offs. The total energy of the η_c candidate was required to be less than 6 GeV to reject e^+e^- annihilation events, which typically have all of the beam energy detected.

For the mass measurement, we required the kaon and pion to be in the tracking volume with best momentum resolution (referred to as good-barrel from now on) ($|\cos\theta| < 0.71$) with high P_T (> 225MeV), since the momenta of low polar angle tracks were not very well measured with our detector. The angle θ is the "polar" angle with respect to the positron beam direction.

4.4. Track Quality Requirements

In addition to the cuts applied to reduce non-two-photon background events, events having neutral particles and the K^0_S selection cuts, we applied additional track quality cuts on all charged tracks. The charged kaon and pion tracks were subjected to track quality cuts which required the tracks to come from the interaction point within 5mm in the r-ϕ plane and 5cm in the r-z plane, and not coming from an identified secondary vertex. All the charged tracks including the charged pion daughters from the K^0_S were required to be corrected for their energy loss in the detector material, not be reconstructed out of residual hits from other tracks in the event, and not be tracks which were at very low polar angles having less than 4 measurements on their z-position (longitudinal direction) in the tracking volume.

4.5. Particle Identification

It is hard to distinguish a high momentum (1-2 GeV) $K^\pm$ from a $\pi^\pm$ using dE/dx or TOF due to their similarity in this momentum range. However, for signal as well as most background events we knew that there had to be another kaon in the event

once a K^0_S was found, to conserve strangeness. Hence, it was not necessary to identify both the remaining tracks. We utilized dE/dx and TOF to identify only the lower momentum track. The produced η_c had a small boost (typical $\gamma\beta$ around 0.3) in the longitudinal direction making one of the tracks (emitted in the backward direction) slow enough to be effectively used for particle identification using dE/dx and TOF. The momentum distributions of the two non-K^0_S tracks in Monte Carlo and data are shown in Figure 7, which show that in majority of the events, the lower momentum track was slow enough to be identified using dE/dx and TOF. In more than 95% of the events, as estimated from Monte Carlo, this identification procedure led to the correct identification of both tracks.

The particle identification (PID) χ^2 value of a track was determined using the measurements from dE/dx and TOF as:

$$\chi^2(PID) = \chi^2_{dE/dx} + \chi^2_{TOF}, \tag{17}$$

where the $\chi_{dE/dx}$ and χ_{TOF} refer to the deviations of the measured dE/dx and TOF from what are expected for the proper mass hypothesis in terms of their resolutions.

Using this combination of dE/dx and TOF for the particle identification, the lower momentum track was identified as a $K^{\pm}$ or a $\pi^{\pm}$ by accepting the lower χ^2 hypothesis. Once a track hypothesis for the lower momentum track was established, it was required that the track be within 3 σ of that hypothesis, using the dE/dx if it was available.

The identities of the tracks in those 5% of events when the event reconstruction failed to make the correct selection are shown in Figure 8 (21: π^+, 22: π^-, 23: K^+, 24: K^-, 11: μ^- and 12: μ^+). Particle ID failed in the momentum range 1-2 GeV, where neither dE/dx nor TOF helped in separating kaon and pion. For the lower momentum track, some muons from kaon decays passed our event selection criteria faking as pions. These low momentum muons could not have been rejected using muon selection criteria, since they were too slow to penetrate the μ counters.

Early on in the analysis, we used to keep two entries per event and weigh each entry according to its PID probability based on the χ^2. This method was eventually discarded, since, as mentioned above, in majority of the events, we could identify the event based on the identity of the lower momentum track, hence there was no need to tackle more book-keeping.

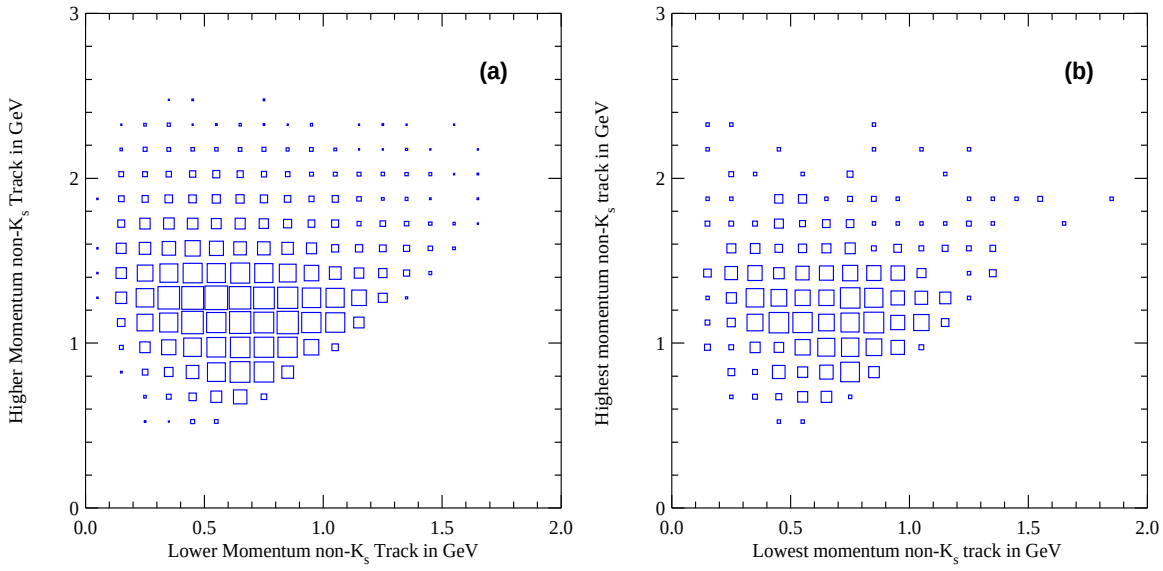

Fig. 7. Momentum distribution of the two non-K_S^0 tracks, in (a) Monte Carlo and (b) data.

4.6. Trigger

As described in the detector section, trigger criteria (trigger lines) are used to reduce the event rate by selecting only interesting physics processes which deal with studies of B and D meson decays. These events typically have high track multiplicity. Trigger requirements are optimized for these events of high track multiplicity by requiring tracks in the barrel part of the detector. These trigger requirements, however, yield low trigger efficiency for two-photon events which generally have low track multiplicity and the final state particles tend to be at low polar angles with respect to the beam direction.

Fortunately, the topology of the $\gamma\gamma$ event depends strongly on the mass of the resonance and the decay mode. Because the η_c is a heavy object, the boost is small. The distribution of the $\gamma\beta$ of the η_c can be seen in Figure 9 (average $\gamma\beta \approx 0.3$). When the η_c decays, it still has many of the tracks in the barrel region, as can be seen in Fig. 14 which shows the distribution of the number of tracks in the good barrel. This has significant implications for the event characteristics and hence triggering issues which depended on finding hits in the barrel TOF and showers in the barrel crystal calorimeter. A massive object like the η_c does not have many of the trigger difficulties associated with light resonances like π^0, η and $\eta^{'}$, where the decay daughters tend to be confined to the endcap region, making it difficult to trigger on them.

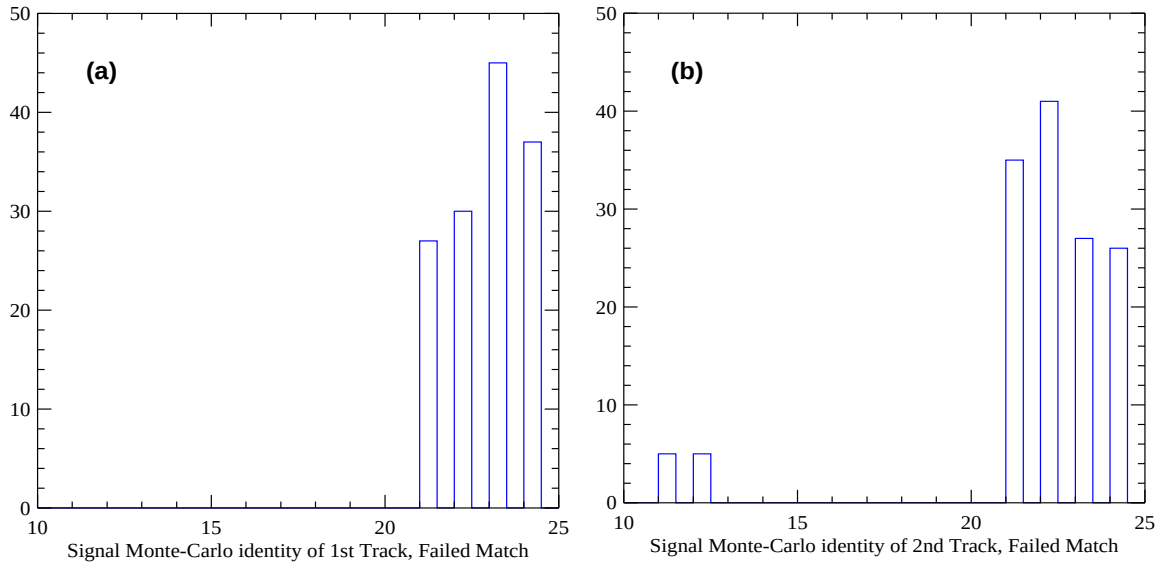

Fig. 8. Identity of the two non-K_S^0 tracks for failed events in signal Monte Carlo events, (a) for higher momentum track and (b) lower momentum track (21: π^+, 22: π^-, 23: K^+, 24: K^-, 11: μ^- and 12: μ^+).

The most efficient trigger lines for our analysis were 2TRK ($\approx 90\%$), BLTHAD ($\approx 75\%$) and TSPHAD ($\approx 60\%$) for events which would pass our analysis cuts. To keep the systematic uncertainty associated with our understanding of the trigger efficiency small, we limited ourself to only one trigger line - the most efficient one for our events, namely the 2TRK trigger which typically required two hits in the barrel time-of-flight counters and a track with more than 340 MeV transverse momentum.

To have a reliable 2TRK trigger-efficiency estimate from the Monte Carlo, we required the event to have at least two high P_T (> 225 MeV) tracks in the good barrel ($|\cos\theta| < 0.71$) and the track with the highest transverse momentum to have at least 350 MeV of P_T so that they would naturally satisfy the 2TRK trigger requirements. In Figure 10, we show the distribution of the number of tracks in the good barrel without and with the requirement of 2TRK trigger, from which one can see the relative dependency of the 2TRK trigger efficiency on the number of tracks in the good barrel.

4.6.1. L3 Software Trigger

It was a goal of the L3 software trigger to reject uninteresting events like beam-related background processes, such as electroproduction on residual gas molecules

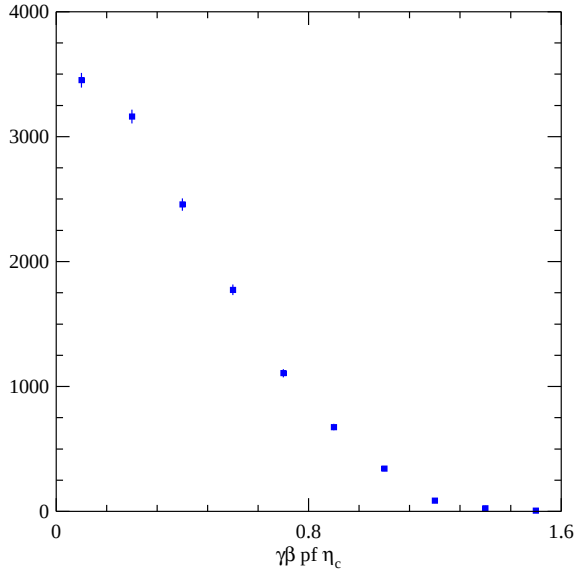

Fig. 9. $\gamma\beta$ distribution of the η_c in Monte Carlo.

and beam-wall interactions, without rejecting too many of useful events like 1 *vs* 1 $\tau\tau$ pairs, two-photon events, or $\mu\mu$ pairs. However, in being able to reject approximately 40% of the uninteresting events, a price had to be paid in terms of rejecting some of the interesting physics events above. The L3 trigger tagged and kept every 8th event it would reject in data so that we could measure the L3 trigger efficiency and study what kind of events were being rejected by this trigger. In Monte Carlo, it tagged and kept all the rejected events. For an event that passed the selection process, L3 tagged it with what criteria (acceptance code) it passed. The L3 trigger primarily depended on two main criteria: BWK (beam-wall killer) tracks and matched energy in the east and west half of the detector. Matched energy requirement demanded that each half of the detector had at least 100 MeV of total energy deposits in the crystals. BWK tracks were those tracks which traveled radially outward from the interaction point with at least, 3 hits on track in the 6 PTL layers, 2 hits in the first 5 VD layers and 3 hits in the next 5 VD layers, for CLEO II. The removal of PTL and addition of the silicon detector in CLEO II.V changed this requirement, since the silicon could not be used for L3 trigger due to being noisy and always producing a track from the noise.

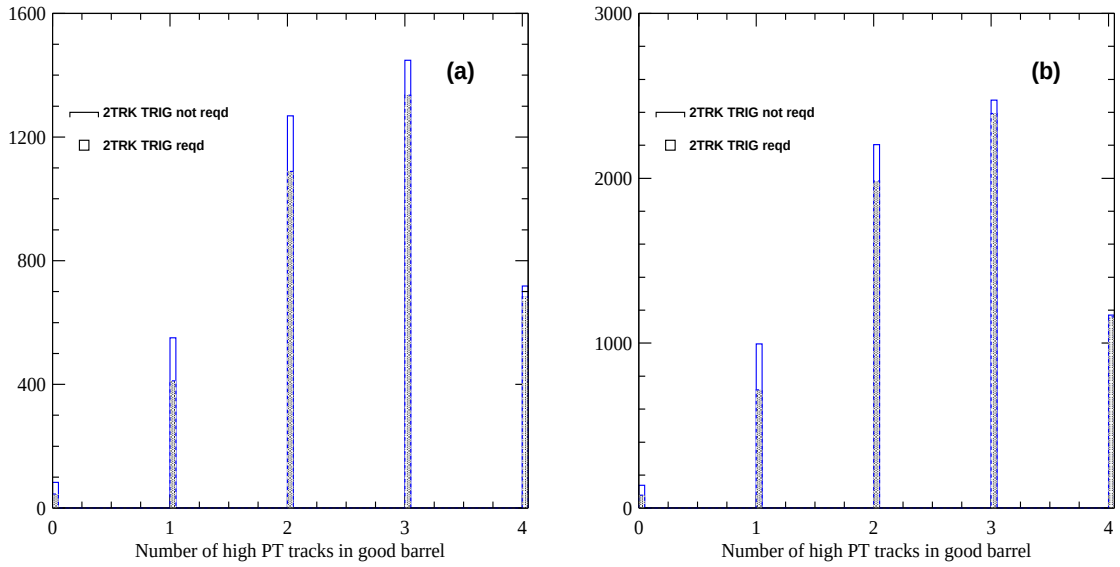

Fig. 10. Distribution of High P_T (> 225 MeV) tracks in Good Barrel and the corresponding distribution requiring 2TRK trigger, for (a) CLEO II and (b) CLEO II.V.

4.7. Special Requirements on Mass Measurement

Tracks which were at low polar angles with respect to the beam direction (high $|\cos\theta|$) were not measured in CLEO as well as the tracks with large polar angles (45 - 135 degrees). The mass measurement accuracy was dominated by the $K^{\pm}$ and $\pi^{\pm}$ tracks because the momentum error of the K^0_S was largely corrected for when the kinematic fit was applied to its decay. Consequently, we required the $K^{\pm}$ and $\pi^{\pm}$ tracks to have minimum P_T (> 225 MeV) and traverse all layers of the tracking volume reaching the good barrel. At the same time, we dropped the requirements that the event satisfy 2TRK trigger, the highest P_T track be greater than 350 MeV and 2 high P_T tracks be in the barrel to recover some of the efficiency loss since they were not essential for good mass measurement.

4.8. Detector Resolution

One of the purposes of our measurements was to determine the total width of the η_c resonance, we needed to understand the detector resolution very well. Requirements to identify the signal events were chosen to keep the resolution better and well understood without losing efficiency too much. For example, to achieve optimum

resolution we required that at least two of the four tracks traverse all layers of the detector volume.

The detector resolutions were obtained from a set of Monte Carlo events generated with the total width of the η_c resonance set to zero. A single Gaussian was not sufficient to describe the reconstructed line shape (mass resolution) representing the detector responses. Hence, a double Gaussian (with the same mean) was used to describe the detector resolution, as shown in Figures 11(b) and 12(b). Comparisons between the single Gaussian and the double Gaussian fits to the detector resolutions are shown in Figures 11 and 12. CLEO II.V had better resolution due to the use of Helium-Propane gas in the tracking devices instead of the argon-ethane gas used for CLEO II. The detector resolutions (width of the narrower Gaussian) measured from Monte Carlo were about 9 MeV for CLEO II and 7 MeV for CLEO II.V. The widths of the wider Gaussian were about 23 MeV for CLEO II and 21 MeV for CLEO II.V. The wider Gaussian accounted for about 20% of the events in both CLEO II and CLEO II.V

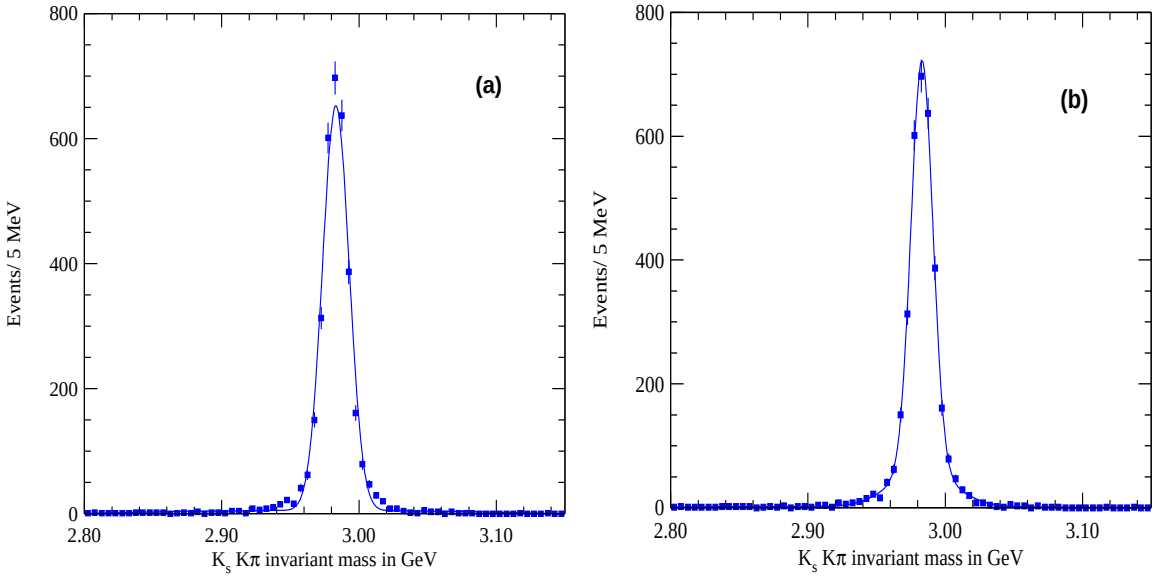

Fig. 11. (a) Single and (b) Double Gaussian fit to the "$\Gamma^{\eta_c}_{tot} = 0$ MeV" CLEO II Monte Carlo.

The double-Gaussian fit to the resolution can be viewed as the combination of a narrow Gaussian that shows the detector resolution, when each track is assigned all the right hits by the track finding program, and the wider Gaussian that represents tracks with some mis-assigned hits. There was also a contribution to the wider Gaussian from events when we assigned $K^{\mp}/\pi^{\pm}$ masses incorrectly. In Figure 13,

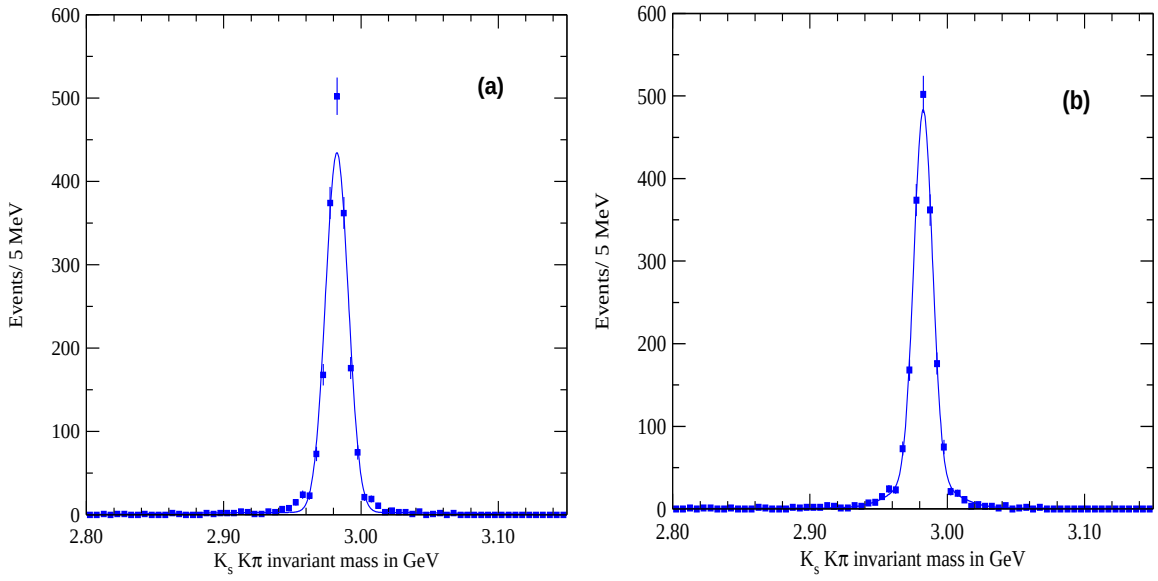

Fig. 12. (a) Single and (b) Double Gaussian fit to the "$\Gamma^{\eta_c}_{tot} = 0$ MeV" CLEO II.V Monte Carlo.

the contribution to the reconstructed width of the candidate from the correct mass assignment ($\approx 95\%$) and incorrect mass assignment ($\approx 5\%$), are shown using Monte Carlo signal events. The wider Gaussian in the fitting absorbed the wide mass distribution due to wrong particle identification, thus leaving the narrower Gaussian representing the most substantial part of the resolution almost unchanged. When we eliminated combinations for which the $K^{\mp}/\pi^{\pm}$ mass assignment was done incorrectly and fit the resulting $K^0_S K^{\mp}\pi^{\pm}$ mass distribution, the width of the narrower Gaussian changed by only around 1%. The contribution of the wider Gaussian went down by around 35% and the wider Gaussian became narrower by about 5%.

With the detector resolution function parameters (σ of the narrow Gaussian, ratio of the widths of the two Gaussians σ_2/σ_1 and ratio of the their respective areas A_2/A_1) found this way, the invariant mass distribution of the η_c candidate was fitted with a Breit-Wigner function describing the natural line shape convolved with the double Gaussian representing the detector resolution.

We generated signal Monte Carlo events assuming that the intrinsic width of the η_c is 27 MeV, and applied our fitting method to test if the generated width could be extracted. Figure 14 show the observed mass distributions for CLEO II and CLEO II.V, respectively. The fit, also shown in the plots, gave widths of (26.8 ± 0.6) MeV and (27.1 ± 0.7) MeV for CLEO II and CLEO II.V, respectively.

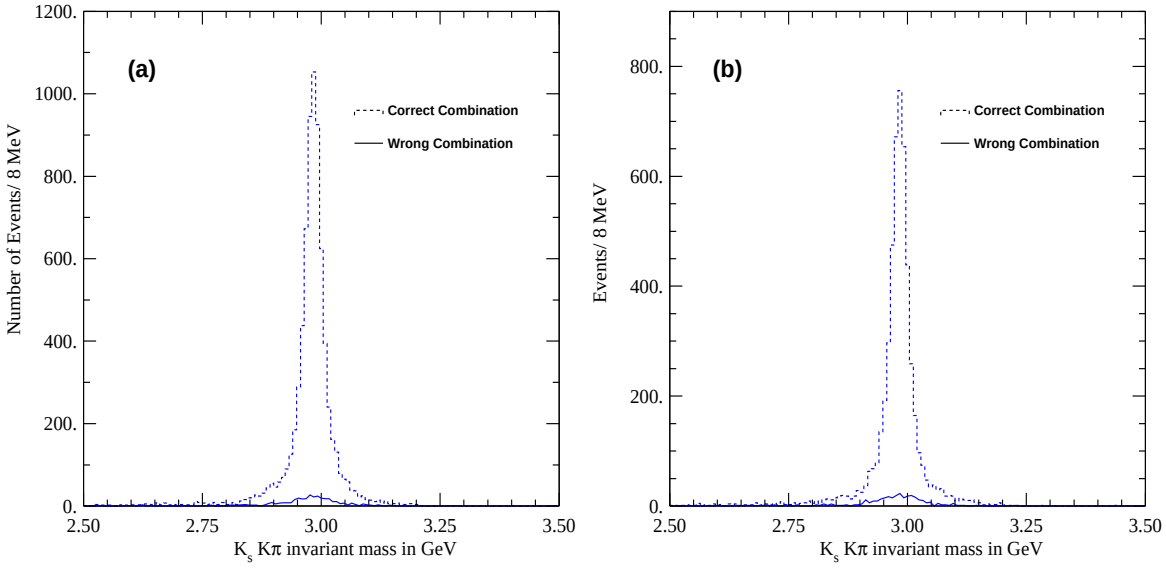

Fig. 13. Contribution to the resolution from correct and incorrect mass assignment of tracks, (a) CLEO II and (b) CLEO II.V.

4.9. Efficiency

The efficiency for individual selection criteria (cut) as estimated from the signal Monte Carlo are presented in Table 1. The efficiencies for the basic requirement cuts are presented in a manner which represents efficiency for each cut when all the previous cuts in the table have already been applied. To obtain the resulting efficiency of all the basic requirements one can multiply the individual efficiencies, *i.e.* $0.38 \times 0.73 \times 0.94 = 0.26$. The efficiencies for the analysis cuts are presented in a manner which represents efficiency for each cut when only the basic requirements cuts have been applied and no other analysis cuts have been applied.

4.10. Expected background from Continuum and Tau Events

The analysis code was run on 16 million continuum $e^+e^- \to \gamma^* \to$ hadrons Monte Carlo events (corresponding to approximately 5fb^{-1}) and 12 million tau-pair $e^+e^- \to \gamma^* \to \tau^+\tau^-$ Monte Carlo events (corresponding to approximately 13fb^{-1}) to estimate the respective background contributions to our processes. Figure 15 shows that the background contribution to our two-photon process from these processes are small. We obtain a contribution of approximately 24 events of the type

Table I. Efficiencies of individual cuts

Cuts Used	**CLEO II (%)**	**CLEO II.V (%)**
Basic Requirements:		
4 Charged Tracks with no net charge	38	34
One K_S^0 Candidate	73	70
Track Quality Cuts for $K^{\mp}$ and $\pi^{\mp}$	94	93
Basic Requirements Efficiency	26	22
Analysis Cuts:		
Transverse Momentum of Candidate (< 0.6 GeV)	90	90
Total Unmatched Neutral Energy (< 0.6 GeV)	94	94
Candidate Energy (< 6 GeV)	100	100
3 σ kaon/pion Consistency	98	98
Two High P_T (> 225 MeV) Tracks in Good Barrel	85	85
Trigger Requirement (any L1/L2)	94	93
2TRK Trigger Requirement	82	84
L3 Trigger	95	91
Highest P_T track with $P_T > 350$ MeV	100	100
Overall Efficiency(all cuts applied)	12.3	8.9

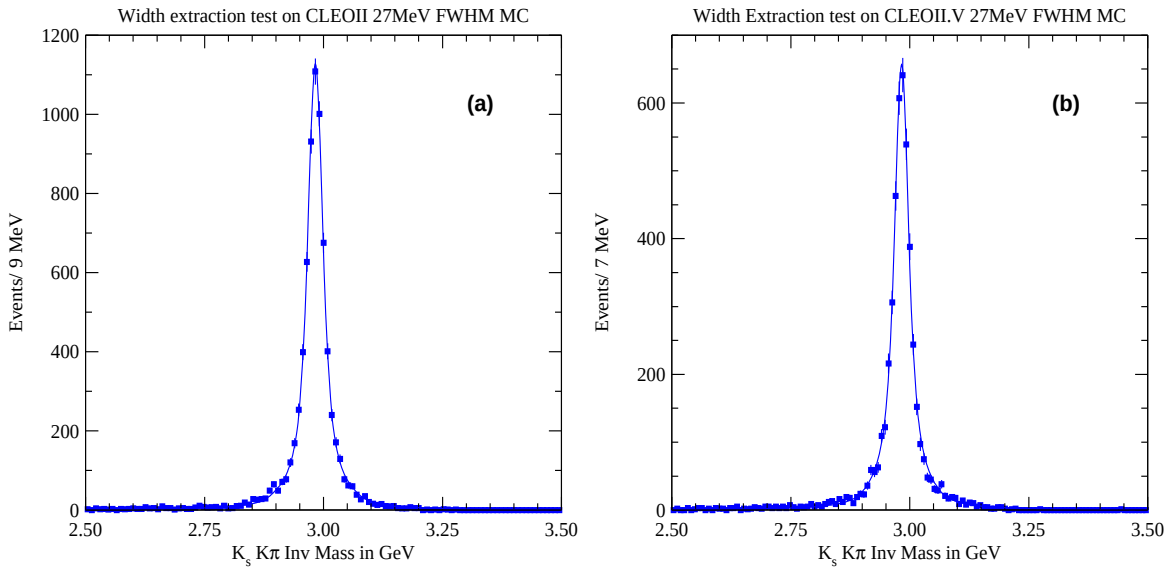

Fig. 14. Width extraction test on Monte Carlo generated with "$\Gamma^{\eta_c}_{tot}$ = 27 MeV" in (a) CLEO II (extracted width = 26.8 ± 0.6 MeV) and (b) CLEO II.V (extracted width = 27.1 ± 0.7 MeV).

$e^+e^- \to \gamma^* \to$ hadrons and approximately 3 events of the type $e^+e^- \to \gamma^* \to \tau^+\tau^-$ in our entire $K^0_S K^{\mp}\pi^{\pm}$ mass range used for fitting, scaled to the CLEO II luminosity. This background level is very small and we expect to have similarly small background in CLEO II.V data. We did not specifically perform CLEO II.V Monte Carlo simulation for these background processes.

5. RESULTS

5.1. Mass Measurement M_{η_c}

The invariant mass distributions, shown in (Figure 16), were fitted to a Breit-Wigner (describing the natural line shape) convolved with a double Gaussian (describing the detector mass resolution) for the signal and a power-law function for the background. The invariant mass distributions for the two datasets were fitted individually and simultaneously, in which we constrained the physical variables, M_{η_c}, $\Gamma^{\eta_c}_{tot}$ and $\Gamma^{\eta_c}_{\gamma\gamma}$ in the two data sets to be the same.

The convolved Breit-Wigner⊗Double Gaussian was parameterized by 6 parameters: number of η_c events, mass of the resonance, total width, σ_1 of the narrower Gaussian of the double-Gaussian resolution function, ratio of the σ of these two

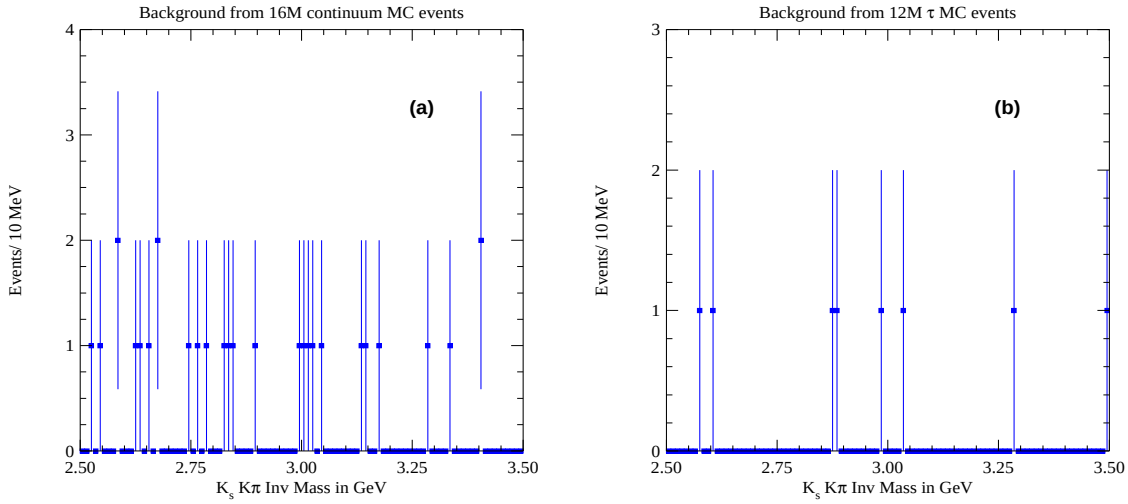

Fig. 15. Selected Events from (a) continuum $q\bar{q}$ and (b) τ processes that pass our analysis cuts.

Gaussians σ_2/σ_1 and their relative area A_2/A_1, where the last 3 parameters were determined from the double-Gaussian fit to the "$\Gamma^{\eta_c}_{tot} = 0$ MeV" Monte Carlo. The background Power-Law function was parameterized as $N_{bg} = A * W^n_{\gamma\gamma}$, where $W_{\gamma\gamma}$ was the two-photon center-of-mass energy for the η_c candidate ($K^0_S K^{\pm}\pi^{\mp}$), and A was a multiplicative normalization factor. The bin widths for fitting the mass distributions in the two data sets were chosen to be approximately equal to the resolution for those data sets. The individual invariant mass fits can be seen in Figure 16 for CLEO II and CLEO II.V data, respectively, whereas the simultaneous fits to the two data sets can be seen in Figure 17. The measured values of M_{η_c} were (2981.6 $\pm$ 3.5) MeV from CLEO II fit, (2979.5 $\pm$ 3.1) MeV from CLEO II.V fit, and (2980.4 $\pm$ 2.3) MeV from simultaneous fit to both the data sets.

5.2. Total Width $\Gamma^{\eta_c}_{tot}$

The total width of the η_c was obtained directly from the Breit-Wigner⊗Double-Gaussian fit to the invariant mass similar to the mass measurement. The data with less restrictive selection criteria were used. The individual fits to CLEO II and CLEO II.V data can be seen in Figure 18, whereas the simultaneous fits can be seen in Figure 19. The measured widths of the η_c were (25.6 $\pm$ 9.4) MeV from CLEO II fit, (26.7 $\pm$

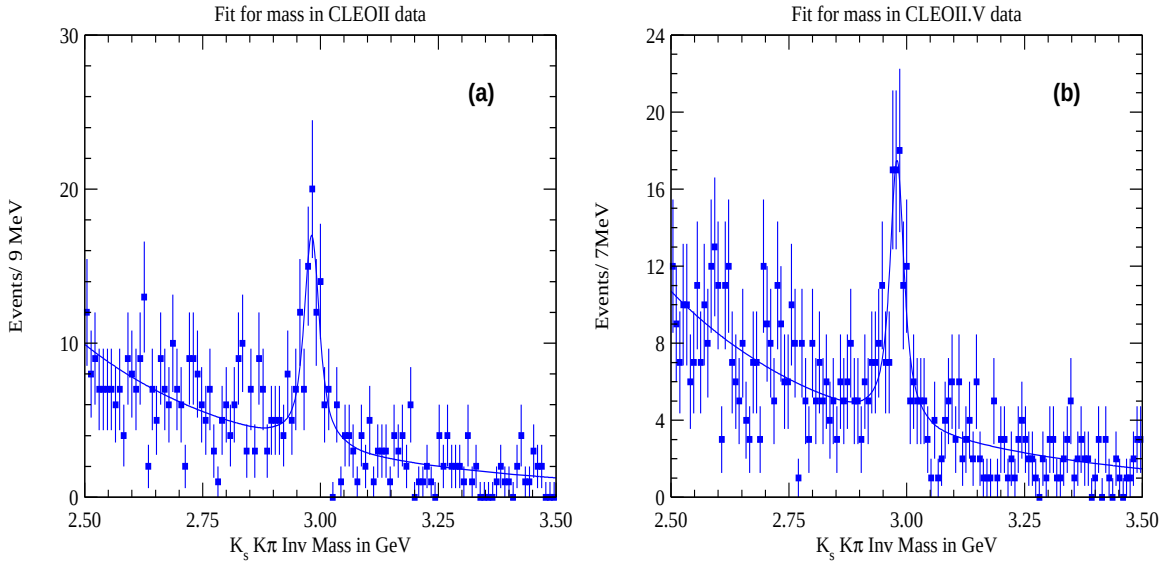

Fig. 16. Mass Measurements from (a) CLEO II (2981.6 ± 3.5 MeV) and (b) CLEO II.V (2979.5 ± 3.1 MeV).

7.3) MeV from CLEO II.V fit, and (27.0 ± 5.8) MeV from the simultaneous fit to both the data sets. The simple weighted average of the CLEO II and CLEO II.V width measurements is (26.3 ± 5.8) MeV, which is 0.7 MeV lower than the measured width from the simultaneous fit to both the data sets (which constrained the 3 measured physical variables - mass, total width and two-photon partial width - in the two data sets to be the same). When we do not apply the constraint of the mass being the same in the simultaneous fit to the two datasets, we obtain a value of (26.3 ± 5.8) MeV for the total width, which is the same as the simple weighted average of the two individual fits. We use the result from the simultaneous fit, where we constrain all the physical parameteres from both the datasets to be the same, but the difference is accounted for as a systematic uncertainty.

5.3. Two-Photon Partial Width $\Gamma_{\gamma\gamma}^{\eta_c}$

The two-photon partial width of the η_c was extracted from the yield in data. This yield was corrected for the detection efficiency and then compared to the expected yield calculated based on the branching fractions $\mathcal{B}(\eta_c \to K_S^0 K^{\mp}\pi^{\pm})$, $\mathcal{B}(K_S^0 \to \pi^+\pi^-)$ and the cross-section $\sigma(e^+e^- \to e^+e^-\gamma\gamma \to e^+e^-\eta_c)$ for a nominal two-photon partial width of 1 keV for the η_c. The cross-section was calculated using the differential

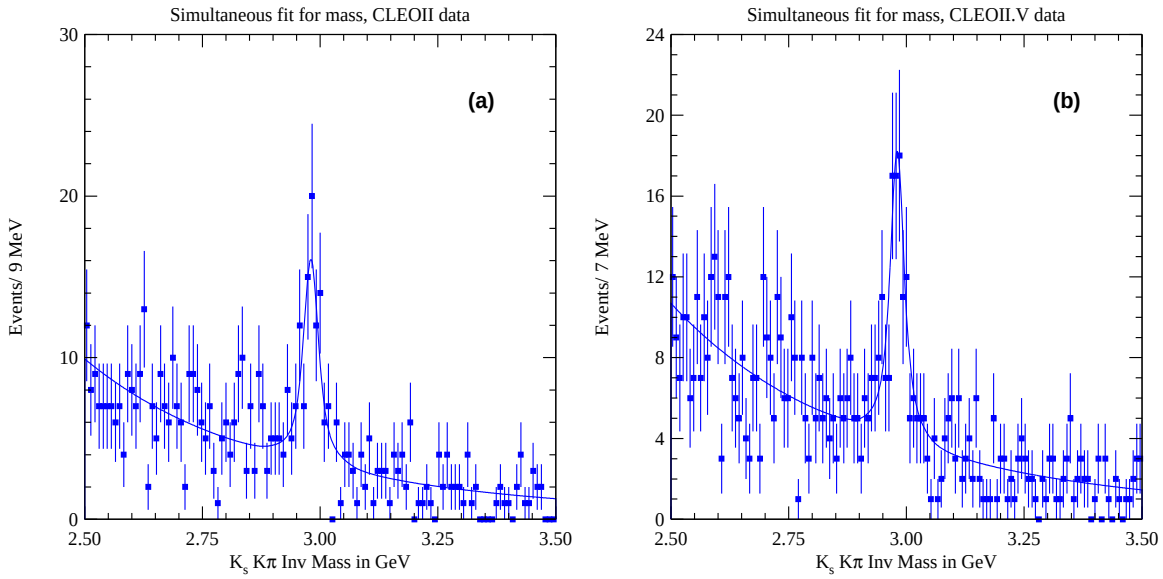

Fig. 17. Mass measurement from simultaneous fit to (a) CLEO II and (b) CLEO II.V; 2980.4 ± 2.3 MeV.

cross-section given in Eq. 9, from the formalism of Budnev *et al.* [13], employing Monte Carlo technique as described in the Appendix C to compute the integral.

This procedure gave us the cross-section for the process $e^+e^- \to e^+e^-\gamma\gamma \to e^+e^-\eta_c$ (integrated over q_1^2 and q_2^2) to be 2.33 pb if $\Gamma_{\gamma\gamma}^{\eta_c} = 1$ keV. The number of expected events was calculated by

$$N = \mathcal{L} \cdot \mathcal{B}(\eta_c \to K_S^0 K^\pm \pi^\mp) \cdot \mathcal{B}(K_S^0 \to \pi^+\pi^-) \cdot \sigma(e^+e^- \to e^+e^-\eta_c) \tag{18}$$

where $\mathcal{L}$ is the luminosity, $\sigma(e^+e^- \to e^+e^-\eta_c)$ is the cross-section mentioned above, $B(\eta_c \to K_S^0 K^\pm \pi^\mp)$ and $B(K_S^0 \to \pi^+\pi^-)$ are the respective branching fractions for the mentioned decays. The values for these variables were

$$\mathcal{L} = 4746\text{pb}^{-1} \text{ for CLEO II and } 8612\text{pb}^{-1} \text{ for CLEO II.V} \tag{19}$$

$$\sigma(e^+e^- \to e^+e^-\eta_c) = 2.33 \text{ pb} \tag{20}$$

$$\mathcal{B}(\eta_c \to K_S^0 K^\pm \pi^\mp) = 1.8\% \tag{21}$$

$$\mathcal{B}(K_S^0 \to \pi^+\pi^-) = 68.6\% \tag{22}$$

where the value of $\mathcal{B}(\eta_c \to K_S^0 K^\pm \pi^\mp)$ was obtained by dividing $\mathcal{B}(\eta_c \to K\bar{K}\pi) = (5.5 \pm 1.7)\%$ quoted in PDG [4] by 3, assuming isospin symmetry for the η_c decay.

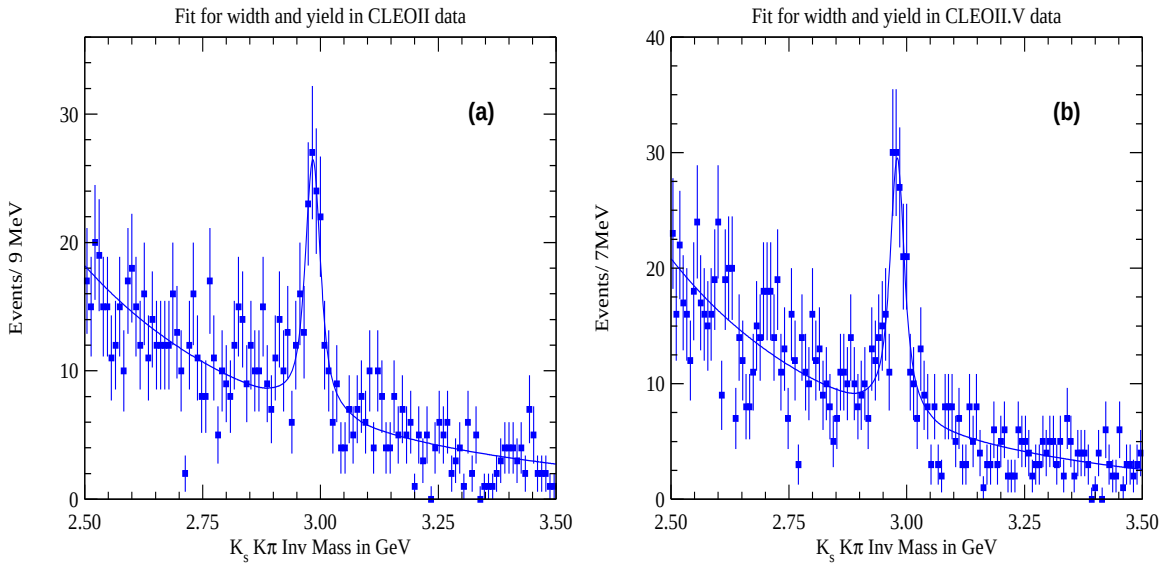

Fig. 18. Yield and Width measurements from (a) CLEO II (130 ± 22 events, 25.6 ± 9.4 MeV width) and (b) CLEO II.V (168 ± 23 events, 26.7 ± 7.3 width).

Using these numbers, the number of expected events for a nominal two-photon partial width of 1 keV were 139 and 253 events for CLEO II and CLEO II.V, respectively. For example, the calculation for expected number of events in CLEO II:

$$N = \mathcal{L} \cdot B(\eta_c \to K_S^0 K^{\pm}\pi^{\mp}) \cdot B(K_S^0 \to \pi^+\pi^-) \cdot \sigma(e^+e^- \to e^+e^-\eta_c) \tag{23}$$

$$\Rightarrow \mathrm{N} = 4746\mathrm{pb}^{-1} \times 2.33\mathrm{pb} \times 1.8 \times 10^{-2} \times 68.6 \times 10^{-2} = 139 \ \text{ events.} \tag{24}$$

Then, from the yield (N_{obs}), the efficiency (ϵ) and the expected number of events for 1 keV $\Gamma_{\gamma\gamma}^{\eta_c}$, we found the actual $\Gamma_{\gamma\gamma}^{\eta_c}$ by the following relationship,

$$\Gamma_{\gamma\gamma}^{\eta_c} = \frac{N_{obs}}{\epsilon \times N} \tag{25}$$

The yields were (130 ± 22) for CLEO II and (168 ± 23) events for CLEO II and CLEO II.V, as seen from Figure 18. The efficiencies, given in Table I, were 12.3% and 8.9% for CLEO II and CLEO II.V respectively. The efficiencies were found by dividing the number of reconstructed signal events from the fit by the number of generated $B(\eta_c \to K_S^0 K^{\pm}\pi^{\mp})$ events, where the K_S^0 decayed to $\pi^+\pi^-$ only (hence, we needed to multiply the $B(\eta_c \to K_S^0 K^{\pm}\pi^{\mp})$ branching fraction with $B(K_S^0 \to \pi^+\pi^-)$ branching fraction while calculating the number of expected events as shown above).

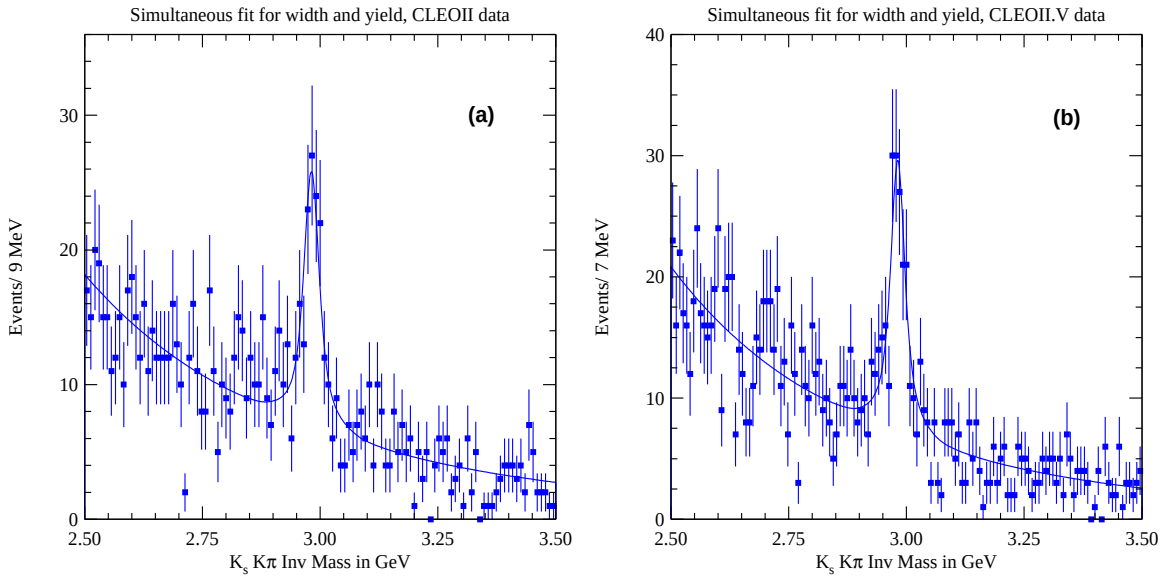

Fig. 19. Yield and Width measurements from Simulataneous Fit to (a) CLEO II and (b) CLEO II.V; 300 ± 32 events, 27.0 ± 5.8 MeV width.

Finally, we got the two-photon partial width of (7.6 ± 1.3) keV for CLEO II and (7.5 ± 1.0) keV for CLEO II.V. For example, the calculation for the two-photon partial width for CLEO II:

$$\Gamma_{\gamma\gamma}^{\eta_c} = \frac{N_{obs}}{\epsilon \times N}, \tag{26}$$

$$\Rightarrow \Gamma_{\gamma\gamma}^{\eta_c} = \frac{130 \pm 22}{0.123 \times 139} = (7.6 \pm 1.3)\text{keV}. \tag{27}$$

The measured $\Gamma_{\gamma\gamma}^{\eta_c}$ from simultaneous fit to the CLEO II and CLEO II.V data sets was (7.6 ± 0.8) keV.

5.4. Ratio of Widths

From our result of the two-photon partial width of the η_c and the PDG average of the e^+e^- partial decay width of the J/ψ, we obtain the ratio of these partial widths to be

$$\frac{\Gamma(\eta_c \to \gamma\gamma)}{\Gamma(\psi \to e^+e^-)} = \frac{7.6 \pm 0.8}{5.3 \pm 0.4} = 1.4 \pm 0.2 \tag{28}$$

The NLO PQCD based calculation, as described in Section 1, predicts this ratio to be approximately 1.6 and it agress well with our experimental ratio.

Table II. Systematic uncertainties in the M_{η_c} measurement.

Source	CLEO II (MeV)	CLEO II.V (MeV)
Mass Calibration of Detector	0.6	0.6
Particle ID	<0.1	<0.1
Signal Shape Parameter	<0.1	<0.1
Overall	0.6	0.6

Similarly, the ratio of our measured two-photon partial decay width and full decay width of the η_c is 3550 $\pm$ 800. This ratio obtained from the NLO PQCD based calculation is approximately 3400 and agress extremely well with our experimentally measured ratio.

6. SYSTEMATIC UNCERTAINTIES

6.1. Systematic Uncertainties in the Measurement of M_{η_c}

The systematic uncertainties in the measurement of M_{η_c} are summarized in Table II. A discussion on the estimation of each of the systematic uncertainty follows. The uncertainties were uncorrelated and added in quadrature to find the combined error.

6.1.1. Mass Calibration

We checked the mass calibration of our detector by measuring the well known masses of heavy particles at the mass scale of the η_c meson like D and J/ψ mesons. Studying the mass calibration of our detector using the D meson was an ideal choice since we had copious production of the D meson in the continuum $q\bar{q}$ process. The measured mass of the $D^{\pm}$ meson in its decay to $K^{\mp}\pi^{\pm}\pi^{\pm}$ final states was (1869.9 $\pm$ 0.1) MeV (Figure 20(b)), to be compared with the PDG average of (1869.3 $\pm$ 0.5) MeV, which does not include CLEO measurements. The measured mass of the J/ψ meson in its decay to e^+e^- and $\mu^+\mu^-$ [18] was (3097.3 $\pm$ 0.2) MeV, to be compared with the PDG average of (3096.88 $\pm$ 0.04) MeV. The measured mass of the $D^{\pm}$ meson

was consistent with the PDG average within the uncertainties and the measured mass of the J/ψ meson was approximately 0.4 MeV or 2σ away from the PDG average. Any systematic effect in the mass measurements needed to be checked and its effect on the η_c mass needed to be estimated. The slightly higher masses measured for the calibrating particles D and J/ψ mesons was an indication that our mass calibration might have been slightly inaccurate.

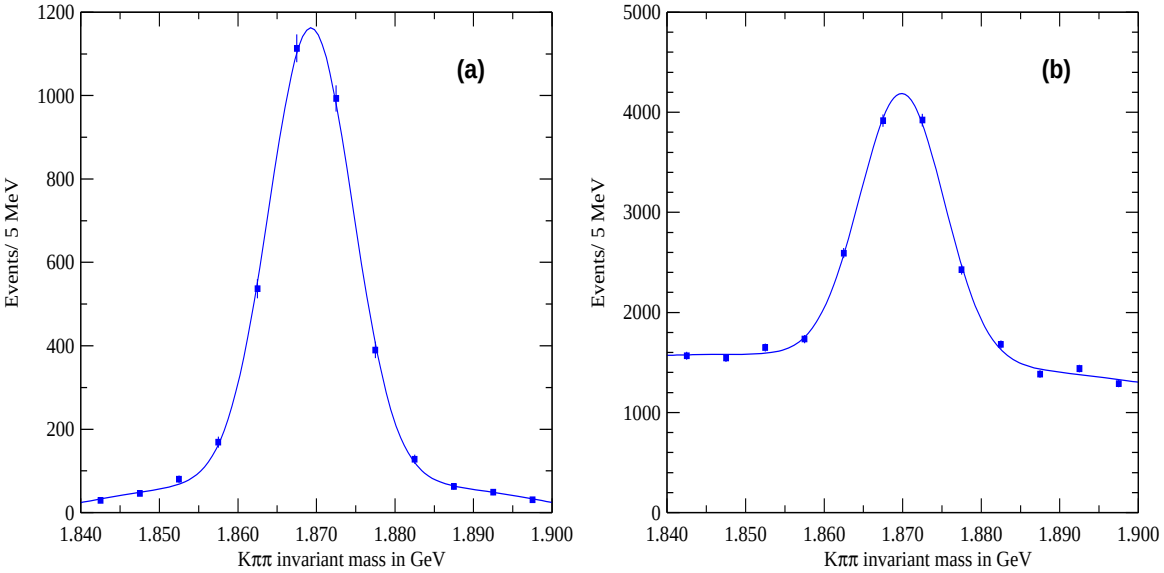

Fig. 20. Single Gaussian Signal + 2nd Order Polynomial Background fit to the invariant mass distributions of $D^{\pm} \to K^{\mp}\pi^{\pm}\pi^{\pm}$ in CLEO II.V (a) Monte Carlo (Mass = 1869.3 ± 0.1 MeV, σ = 5.32 ± 0.10 MeV) and (b) data (Mass = 1869.9 ± 0.1 MeV, σ = 5.36 ± 0.12 MeV).

In addition, with a proper calibration, we expect that the invariant mass of an object should show no systematic variation with respect to any variable under observation. However, as one can see in Figure 21(a), the invariant mass of the $D^{\pm}$ meson had a definite variation with its polar angle $\theta_{D^{\pm}}$ with respect to the beam direction.

We found that this mass shift was correlated to the direction of the final state particles that the $D^{\pm}$ decayed into. When at least one of the daughter tracks ($K^{\mp}$, $\pi^{\pm}$ or $\pi^{\pm}$) moved in the direction of the endcaps ($|\cos\theta_{D^{\pm}}| > 0.71$), the measured $D^{\pm}$ mass was higher. However, we could not identify the exact mechanism of this phenomenon.

Figure 21(b) shows the variation of the measured $D^{\pm}$ mass with the cosine of the polar angle of the kaon ($\cos\theta_{K^{\mp}}$) when the two pions were in the good-barrel acceptances ($|\cos\theta_{\pi^{\pm}}| < 0.71$). The measured $D^{\pm}$ mass was constant until the kaon went outside the good-barrel region ($|\cos\theta_{K^{\mp}}| > 0.71$). We tested this hypothesis on

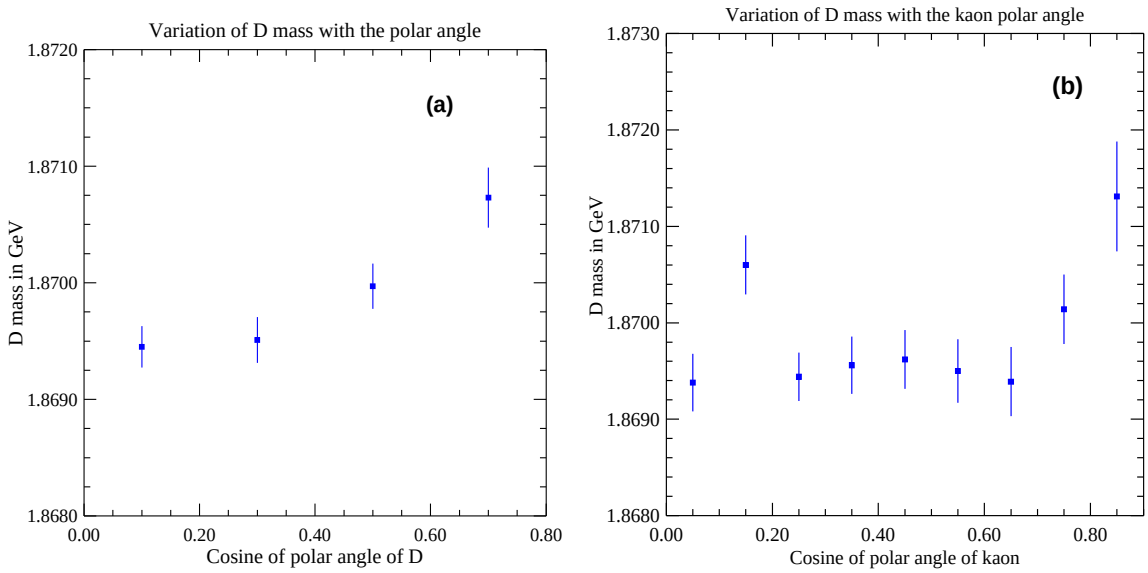

Fig. 21. Variation of the $D^{\pm}$ mass with polar angle of (a) the $D^{\pm}$ direction and (b) the $K^{\mp}$ direction.

mass measurement of the D^0 meson in its decay to $K^0_S\pi^{\pm}\pi^{\mp}$, where the D^0 mesons came from the B meson decays. The results can be seen in Figure 22, where the first plot shows the mass measurement without any requirements on the daughter track directions and the second plot shows the mass measurement when the two daughter pions were measured to be in the good barrel with minimum P_T of 225 MeV. The mass of the D^0 meson was (1865.0 $\pm$ 0.2) MeV when we did not require the daughter pions to be in the good barrel (Figure 22(a)), and (1864.6 $\pm$ 0.3) MeV when we required the daughter pions to be in the good barrel with minimum P_T of 225 MeV (Figure 22(b)). The latter measurement was in excellent agreement with the PDG average of (1864.6 $\pm$ 0.5) MeV. In fact, we measured the D^0 mass when both the charged pions were outside the good-barrel acceptances and obtained a value of (1865.5 $\pm$ 0.4) MeV (Figure 23), which was about 0.9 MeV ($\approx 1.5\sigma$) higher than the PDG average. We made a similar study using $J/\psi \rightarrow \mu^+\mu^-$. The measured J/ψ mass was slightly higher than the PDG value as mentioned above. However, when the μ^+ and μ^- were required to be in the good barrel acceptances the measured J/ψ mass was (3096.7 $\pm$ 0.2) MeV, consistent with the PDG average of (3096.88 $\pm$ 0.04) MeV within the errors, as shown in Figure 24. When one of the daughter muons from the J/ψ decay went in the direction of the endcaps, the measured mass was higher (3098.6 $\pm$ 1.1) MeV. These measurements motivated us in our mass measurement of the η_c meson to limit ourselves to only those events where the daughter charged kaon

and charged pion were in the good-barrel acceptances with minimum P_T of 225 MeV. Various CLEO calibrations had been extensively tested for tracks in the good-barrel acceptances, whereas the momentum calibration for tracks outside the good-barrel acceptances was not.

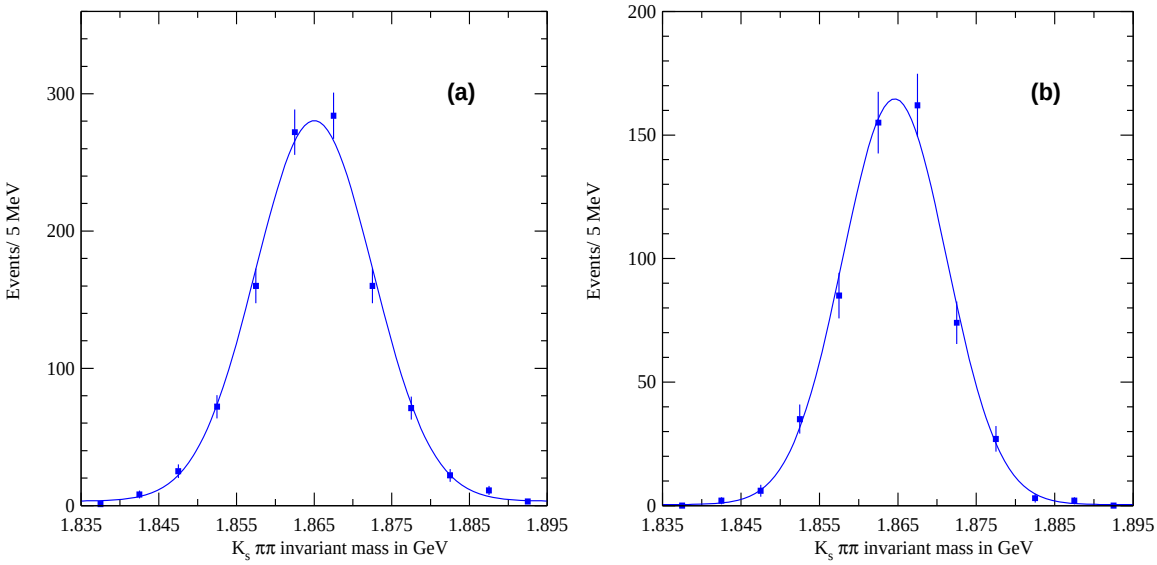

Fig. 22. Single Gaussian Signal + Constant Background fit to the invariant mass distributions of $D^0 \to K^0_S \pi^\pm \pi^\mp$, (a) without any requirements on charged pions (Mass = 1865.0 $\pm$ 0.2 MeV, σ = 7.6 $\pm$ 0.2 MeV) and (b) with requirements on charged pions to be in good-barrel (Mass = 1864.6 $\pm$ 0.3 MeV, σ = 6.6 $\pm$ 0.3 MeV).

In general, inaccurate mass calibration can result from inaccurate description of the detector material which is used to make ionization energy loss correction for tracks traversing them or from inaccurate calibration of the magnetic field which determines the momenta of the tracks. It was hard to disentangle the effects due to material and magnetic field on the momentum measurements. Over the years, CLEO had used the mass measurements of the D and J/ψ mesons to calibrate the detector. We estimated the effects of varying the assumed amount of the detector material as well as varying the assumed magnetic field strength on the measured mass of the $D^\pm$ meson and extrapolated their effect to the η_c mass to assign a systematic uncertainty due to the mass calibration of our detector.

To study the effect of assuming more (or less) material on the mass measurement of the $D^\pm$ meson, we made each daughter track ($K^\mp$, $\pi^\pm$ and $\pi^\pm$) of the D meson go through more (or less) material by performing a dE/dx energy loss correction to the track momentum using the Bethe-Bloch equation[19]. We studied the variation

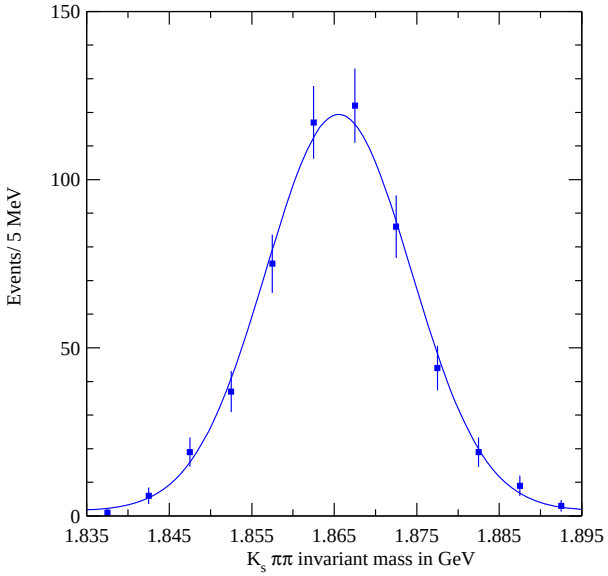

Fig. 23. Single Gaussian Signal + Constant Background fit to the invariant mass distributions of $D^0 \to K^0_s \pi^{\pm}\pi^{\mp}$, when both the daughter pions are outside the good-barrel acceptances (Mass = 1865.5 ± 0.4 MeV, σ = 8.8 ± 0.5 MeV).

in the measured mass of the $D^{\pm}$ meson with the variation in the amount of dE/dx energy loss correction due to the changing amount of detector material. The changes in the detector material was assumed to be concentrated in the inner section of the detector to maximally affect the performed energy correction. The results are shown in Figure 25(a). Figure 25(b) shows a similar plot for the η_c mass.

Since the mass calibration of our detector was performed using the $D^{\pm}$ meson whose world average has an uncertainty of ± 0.5 MeV, we adopted a conservative approach to assign the systematic uncertainty on the measured η_c mass. We estimated how much change in the amount of material was needed for our measured mass of the $D^{\pm}$ meson to start disagreeing with the corresponding PDG average by more than 1.5σ (0.75 MeV). The change in the amount of material needed for this level of disagreement was approximately ± 0.25 g/cm^2, which produced a variation of ±0.6 MeV in the measured η_c mass.

A similar change in mass could also be achieved by changing the absolute scale of the magnetic field. The absolute scale of the magnetic field was changed (by approximately 6×10^{-4}) to result a shift of 0.75 MeV in the measured $D^{\pm}$ mass and the η_c analysis was redone with this new magnetic field. This produced a correction of approximately 0.6 MeV to the η_c mass, similar to the result obtained from the variation of the detector material.

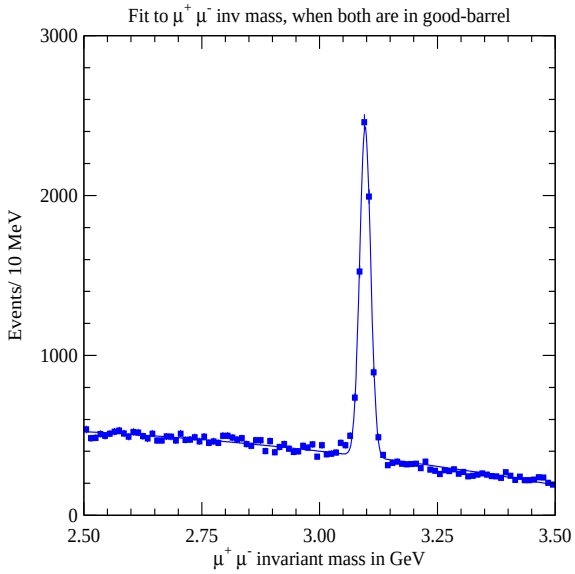

Fig. 24. Single Gaussian Signal + 2nd Order Polynomial Background fit to the invariant mass distribution of $J/\psi \to \mu^+\mu^-$, where both the muons are in the good-barrel region (Mass = 3096.7 ± 0.2 MeV).

We assigned a 0.6 MeV systematic uncertainty in the η_c mass due to possible uncertainty in the mass calibration of our detector.

6.1.2. Particle ID

By mis-identifying a daughter particle and hence mis-assigning the mass to the daughter particle, it is possible to change the reconstructed mass of the parent particle. In the case of the η_c decay, a kaon mis-identified as a pion would move the measured η_c mass down and a pion mis-identified as a kaon would move the measured η_c mass up. As described in Section 4.8 on detector resolution, the effect of the particle mis-identification leads to a broadening of the wider Gaussian of the double-Gaussian resolution function and the corresponding increase in the relative area of the wider Gaussian. We estimated the effect of this mis-identification on the mass measurement of the η_c by changing the fraction of mis-identified events by varying the relative area of the two Gaussians describing the detector resolution. *A priori*, since the mass distribution for the mis-identified events was not biased towards either side of the mass peak and only had a broad distribution centered around the true η_c mass (Figure 13), we did not anticipate any substantial change in the mass due to the variation in the fraction of mis-identified events in the selected events. The results

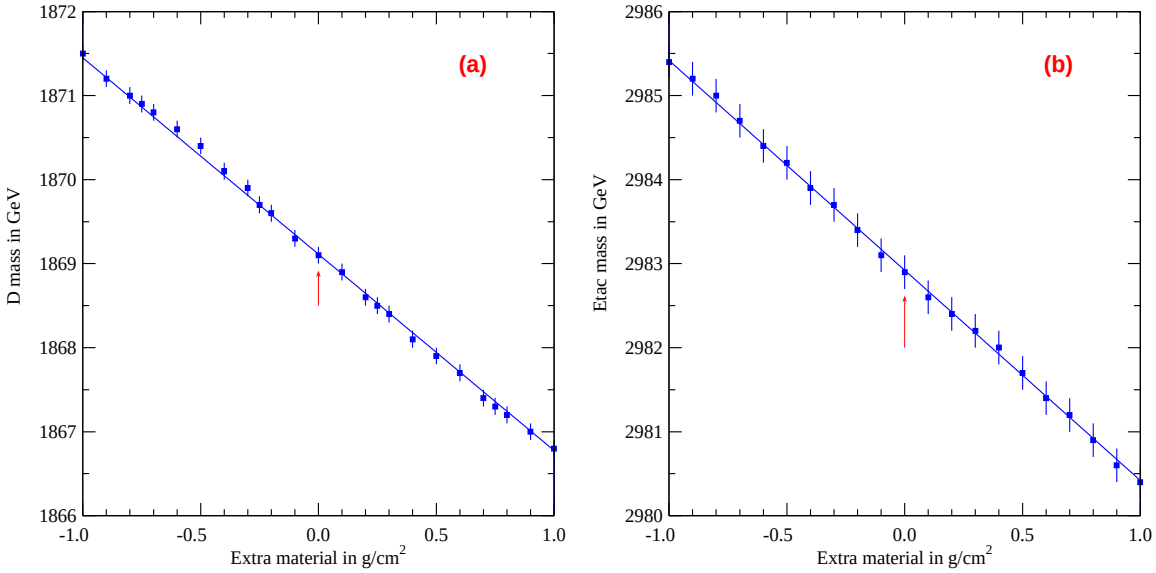

Fig. 25. Dependence of the calculated mass on the amount of addition or reduction of material from the assumed amount of detector material for (a) the $D^{\pm}$ and (b) the η_c.

Table III. Effect of particle misidentification on the η_c mass measurement.

PID fakes	δM in MeV, CLEO II	δM in MeV, CLEO II.V
Nominal fake rate	0.00	0.00
Double fake rate	+0.07	0.00
No fake	-0.07	0.00

from the measurements of the η_c mass with different fractions of mis-identified events (fakes) are summarized in Table III.

As expected, we found that there was no systematic shift in the measured η_c mass due to the particle mis-identification. We did not assign any systematic uncertainty to the mass measurement due to possible uncertainties in the particle identification procedure.

6.1.3. Background Function

In our fitting procedure we allowed the shape of the background to be a free parameter. The possible uncertainty in the measured mass of the η_c due to variations

in the power of the background was included in the statistical uncertainty. The two-photon cross-section is expected to be described by a power law behavior in the invariant mass variable away from the production threshold [12]. We did not assign any additional systematic uncertainty due to possible uncertainties in the shape of the background beyond what was incorporated by the fitting procedure as part of the statistical uncertainty.

6.1.4. Signal Shape Parameter

We estimated the effect of the variation of the signal shape parameters on the measured mass in the data. The effect of variation in the width of the narrower Gaussian on the measured mass in data had already been accounted for as part of the statistical uncertainty in the fit. The modeling of the other two shape parameters, σ_2/σ_1 and A_2/A_1, in the Monte Carlo had been compared with data [20] in the case of the D meson decays by comparing the signal shape variables in Monte Carlo and data and had been found to be consistent within 15%. We allowed the signal shape parameters to vary within this 15% uncertainty to measure any shift in the η_c mass. The effect of changing the relative width and area of the two Gaussians did not change the position of the mass peak. We did not assign any systematic uncertainty to the measured mass due to possible uncertainties in the parameters with which we fitted the signal shape.

6.1.5. Interference

Interference between the resonant and non-resonant $K^0_S K^{\mp}\pi^{\pm}$ final state amplitudes can shift the apparent mass of the η_c resonance away from its true mass. The extent of this shift in the measured mass depends on the fraction of the final states that interferes with the final states that the η_c decays into. Interference is possible when the quantum numbers of the final states are the same. In non-resonant two-photon events, final states of natural parity are predominantly produced in comparison to final states with unnatural parity [12]. Hence the fraction of non-resonant events with the same parity as that of the η_c (0^-) is expected to be small and thus the possibility of interference is also expected to be small.

Table IV. Systematic uncertainties in the $\Gamma_{tot}^{\eta_c}$ Measurement.

Source	CLEO II (MeV)	CLEO II.V (MeV)
Detector Resolution	0.3	0.3
Particle ID	1.3	1.3
Mass Calibration	0.7	0.7
Signal Shape Parameter	0.5	0.5
Overall	1.6	1.6

We ignore the possibility of interference and do not take into account any systematic shift in the measured mass of the η_c due to interference.

6.2. Systematic Uncertainties in the Measurement of $\Gamma_{tot}^{\eta_c}$

The systematic uncertainties in the measurement of $\Gamma_{tot}^{\eta_c}$ are summarized in Table IV. A discussion on the estimation of each of the systematic uncertainty follows. The uncertainties were uncorrelated and added in quadrature to find the combined error.

6.2.1. Detector Resolution

The reliability of the Monte Carlo to simulate the detector resolution was checked by studying the decay $D^{\pm} \to K^{\mp}\pi^{\pm}\pi^{\pm}$ in Monte Carlo and data. The choice of $D^{\pm}$ was made since it has almost no intrinsic width (the width we see in data is primarily due to the detector resolution), and also because it has a 3 body decay that produces momentum distributions of the daughter particles similar to our $\eta_c \to K_S^0 K^{\mp}\pi^{\pm}$ decay. We used the CLEO II.V datasets for this study. Fits to the invariant mass distributions in Monte Carlo and data are shown in Figure 20. The detector resolution measured from CLEO II.V Monte Carlo was (5.32 $\pm$ 0.10) MeV and that measured from CLEO II.V data was (5.36 $\pm$ 0.12) MeV. They were consistent with each other. A study [20] with the CLEO II data had shown similar agreement between the detector resolution predicted by the Monte Carlo simulation and that measured in the data.

To give a conservative estimate of the uncertainty in the measured η_c decay width, we estimated how much change in the multiple scattering component of the resolution was allowed before the Monte-Carlo predicted resolution and the resolution measured in data for the $D^{\pm}$ meson started disagreeing at the 1.5σ level. As described in the mass systematics section, there was a possibility of discrepancy in our knowledge of the amount of detector material inside the tracking volume.

The change in the detector resolution required before the reconstructed $D^{\pm}$ width in Monte Carlo and data started disagreeing at 1.5 σ level was $\approx 3\%$ (≈ 0.15 MeV) of the total detector resolution. The total detector resolution was dominated by the contribution from multiple scattering and position measurement errors, which could be added in quadrature to obtain the total resolution. The effect on the measured detector resolution due to uncertainties in either of these two parameters was similar. Hence, we can focus on uncertainties in either of these two parameters. Subtracting in quadrature the resolution due to the position measurement errors, the change in multiple scattering was limited to $\approx 4\%$ of the total width. The multiple scattering goes as the square root of the extra detector material (Molière theory)[21]. From this we deduced that the maximum material change was limited to $\approx 8\%$ of the total inner detector material.

Using the allowed variation in the knowledge of the amount of detector material above we found that the maximum variation in the detector resolution of the η_c mass due to multiple scattering was $\approx 4\%$ and correspondingly the error in the total η_c resolution being limited to $\approx 2\%$ (≈ 0.2 MeV). We changed the width of the narrower of the two Gaussians describing the detector resolution of the η_c decay in the fitting procedure by $\pm$ 2% to study the effect on the measured decay width. This study gave rise to a maximum of $\pm$ 1% (≈ 0.3 MeV) change in the measured total decay width in CLEO II and CLEO II.V. We assigned 0.3 MeV as the systematic uncertainty on the total decay width of the η_c meson due to uncertainty in the detector resolution.

6.2.2. Particle Identification

The procedure for event selection and track identification using our particle identification procedure assigned wrong masses to the charged kaon and charged pion in about 5% of the η_c events and it led to a wider distribution, as described in Section 4.8 (Figure 13). The wider distribution of the mis-identified events left the narrower

Table V. Effect of Particle Mis-identification on the η_c Width Measurement.

PID fakes	σ_1(II)	$\frac{S_2}{S_1}$(II)	$\frac{A_2}{A_1}$(II)	$\Gamma_{tot}^{\eta_c}$(II)	σ_1(II.V)	$\frac{S_2}{S_1}$(II.V)	$\frac{A_2}{A_1}$(II.V)	$\Gamma_{tot}^{\eta_c}$(II.V)
Nominal Fakes	9.07	5.89	.12	25.6	7.46	5.82	.13	26.7
Double Fakes	9.19	6.14	.16	24.3	7.59	5.91	.17	25.4
No Fakes	8.93	5.15	.08	26.7	7.33	5.50	.09	28.0

Gaussian of the resolution function almost unchanged and only changed the relative width and area of the two Gaussians, namely σ_2/σ_1 and A_2/A_1. To estimate the effect of uncertainties in the particle identification procedure, we varied the contribution of the wider Gaussian in the double-Gaussian resolution function using the following procedure.

We doubled the fraction of the mis-identified events (we call them fakes in the tables) in the "$\Gamma_{tot}^{\eta_c} = 0$ MeV" Monte Carlo, from which we estimated the signal shape parameters. As expected, the narrower Gaussian did not change appreciably and the contribution of the wider Gaussian to the total area became more. When we used these new shape parameters, which were obtained by assuming our particle mis-identification was twice worse, the measured width of η_c from data were (24.3 $\pm$ 9.2) MeV for CLEO II to be compared with the nominal measurement of (25.6 $\pm$ 9.4) MeV. Similarly for CLEO II.V, the new measurement resulted in the width of η_c as (25.4 $\pm$ 7.2) to be compared with the nominal measurement of (26.7 $\pm$ 7.3) MeV. The wider Gaussian, by having a higher value of σ_2/σ_1 and A_2/A_1 absorbed part of the Breit-Wigner tail and resulted in the measured width being smaller by about 5% in both CLEO II and CLEO II.V.

Similarly, when we assumed that there were no mis-assignment of masses to the charged kaon and charged pion, the widths of η_c extracted from the data were (26.7 $\pm$ 9.5) MeV and (28.0 $\pm$ 7.4) MeV for CLEO II and CLEO II.V, respectively. The Breit-Wigner absorbed a part of the background as its own tail and resulted in the measured width being higher by about 5% in both CLEO II and CLEO II.V.

We assigned a 5% systematic uncertainty on the measured total width of the η_c meson due to possible uncertainties in the particle identification process, in both CLEO II and CLEO II.V. Summary of the above tests are given in Table V.

6.2.3. Mass Calibration

The individual mass-measurement fits to the invariant mass distributions obtained from the CLEO II and CLEO II.V datasets produced results of (2981.6 ± 3.5) MeV and (2979.5 ± 3.1) MeV, respectively. This indicates that the two detector configurations CLEO II and CLEO II.V have mass calibration off by about 2 MeV at the η_c mass scale. While obtaining the total width from the simultaneous fits to the two datasets, by constraining the masses in the two datasets to be the same, we obtain a value (27.0 ± 5.8) MeV which is 0.7 MeV higher than the simple weigthed average (26.3 ± 5.8) MeV of the two individual fits. We assigned this discrepancy of 0.7 MeV as a systematic uncertainty in the measured total width.

6.2.4. Background Function

For the reasons discussed in Section 6.1.3, we did not assign any additional systematic uncertainty to the measured total width of the η_c due to possible uncertainties in the shape of the background.

6.2.5. Signal Shape Parameter

Similar to the study described in Section 6.1.4 on estimation of the systematic uncertainty in M_{η_c} due to the variation in the signal shape parameters, we studied the effects of variation in the signal shape parameters on the measured width. We did not do any variation on the narrower Gaussian of the resolution, since that variation had already been accounted for in the systematic uncertainty estimate from uncertainties in the detector resolution. We summarize the results in Table VI.

The measured width did not change noticeably ($< 0.5\%$) due to the change in σ_2/σ_1 (which signifies the difference in the amount of mis-measurement and mis-assigned hits on tracks) and changed by about ± 2% both in CLEO II and CLEO II.V due to the change in A_2/A_1 (which signifies the change in the probability of mis-assigned hits on tracks). We added the uncertainties in quadrature and assigned a 2% systematic uncertainty to the total width measurement due to uncertainties in the signal shape parameters in both CLEO II and CLEO II.V.

Table VI. Effect of Signal-shape Variation on the η_c Width Measurement.

Shape Parameter	$\Gamma^{\eta_c}_{tot}$ MeV (II)	$\Gamma^{\eta_c}_{tot}$ MeV (II.V)
Nominal	25.6	26.7
σ_2/σ_1 +15%	25.6	26.7
σ_2/σ_1 -15%	25.5	26.8
A_2/A_1 +15%	25.1	26.1
A_2/A_1 -15%	26.0	27.2

6.2.6. Interference

We discussed in section 6.1.5 the possible effects of interference on the measured η_c mass and why we ignore it. Similarly, we ignore the possible effects of interference on the measured total width of the η_c, since we expect majority of the non-resonant final states to have different parity than the parity of the η_c. We do not assign any systematic uncertainty to the measured total width due to possible interference between the final states.

6.2.7. Consistency Check

We applied restrictive particle identification criteria to observe the resulting change in the η_c width measurement. In our nominal analysis, we required the lower momentum track to be 3σ consistent with its chosen hypothesis using dE/dx. We changed this requirement to 2σ and 1σ consistency levels to measure the total width. The results of this test were consistent with each other and are summarized in Table VII. These changes are within the estimated systematic error.

6.3. Systematic Uncertainties in the Measurement of $\Gamma^{\eta_c}_{\gamma\gamma}$

The systematic uncertainties in the measurement of $\Gamma^{\eta_c}_{\gamma\gamma}$ are summarized in the Table VII. A discussion on the estimation of each of the systematic uncertainty follows. The uncertainties were added in quadrature to find the combined error.

Table VII. Consistency Check on the η_c Width Measurement.

dE/dx Consistency	$\Gamma_{tot}^{\eta_c}$ MeV (II)	$\Gamma_{tot}^{\eta_c}$ MeV (II.V)	$\Gamma_{tot}^{\eta_c}$ MeV (simultaneous fit)
Nominal (3σ)	25.6	26.7	27.0
2 σ	24.4	23.3	24.8
1 σ	25.2	25.7	25.9

Table VIII. Systematic uncertainties in the $\Gamma_{\gamma\gamma}^{\eta_c}$ measurement.

Source	CLEO II (%)	CLEO II.V (%)
Luminosity	1	1
Form Factor	$< .5$	$< .5$
Trigger (L0)	1	1
Trigger(L1/L2)	2	1.5
Trigger(L3)	1.5	3
Tracking	1	1
K_S^0 Efficiency	1	1
Sub Resonance in η_c Decay	1	1
Feed-down from higher States	$< .5$	$< .5$
Detector Resolution	$< .5$	$< .5$
Particle ID	2	2
Signal Shape Parameter	1.5	1.0
Overall	5.0	5.0

6.3.1. Luminosity and $e^+e^- \to e^+e^-\eta_c$ Cross-section

The uncertainty on the integrated luminosity was taken to be 1% [22]. The production cross-section for η_c from the process $e^+e^- \to e^+e^-\eta_c$ was taken as the average cross-section obtained from generating Monte Carlo in many run numbers distributed over all the data sets, with the beam energy (which influences the calculated cross-section) for a particular run taken as the actual beam energy for that data run. We did not assign any systematic uncertainty to the cross-section, except through the form-factor, since the QED part of the cross-section is very well understood and we used the full cross-section equation for the process $e^+e^- \to e^+e^-\eta_c$ as given by Budnev *et al.* [13].

6.3.2. Form Factor

The expression for the form factor has two uncertainties: functional dependence of the form factor on the q^2 values and the exact value of the pole mass. The choice of the models of q^2 dependence of the form factor did not contribute any appreciable systematic uncertainty to our untagged two-photon analysis since the photons were almost real and the q^2 values of the two photons were close to zero. We did not assign any systematic uncertainty due to the model uncertainty in the q^2 dependence of the form factor.

To estimate the systematic uncertainty due to the uncertainty in the pole mass, we went to the extreme of assuming a form factor of unity (infinite pole mass) and generated Monte Carlo. The effect was through changing the P_T distribution of the η_c (due to change in the differential cross-section with P_T) which would effect total cross section and the efficiency of the P_T cut in the analysis. However, a priori, we knew that the P_T dependence primarily came from the photon propagators in the cross-section in low q^2 regime and we did not expect to see much effect until we went to very high q^2 values. From the result obtained from this new Monte Carlo generated with a unity form factor (infinite pole mass) the change in efficiency was 0.2%. We did not assign any systematic uncertainty due to possible uncertainty in the form factor. Recent results from LEP indicate that the pole mass for the $\eta_c\gamma\gamma$ form factor is most likely that of the J/ψ meson mass [23], we did not go to the other extreme of using the ρ meson mass as the pole mass. Theoretically, the corresponding differential

cross section would be suppressed by at least a factor of $(\alpha_s/\pi)^3$, due to the three gluon coupling [2].

6.3.3. Tracking Efficiency

Jon Urheim [24] had done a study of track finding efficiency using the process $e^+e^- \to \tau^+\tau^-$, where one τ decayed leptonically and the other τ decayed to three charged pions plus neutrals. The efficiency measurement was based upon identifying the lepton and two of the pions, and then determining whether a track for the third pion was found. The track was required to be of "good quality" in terms of r.m.s distance from the track to individual hits, the closest approach of the track to the nominal primary interaction point, etc. This study had found that the Monte-Carlo predicted track finding efficiency for high momentum tracks in the barrel acceptances was good to 0.1% level, and 0.5% for low momentum particles with momentum 100-200 MeV. Only a small fraction (less than 15%) of our events had at least one track momentum below 200 MeV. Conservatively, we assigned a 1% systematic uncertainty for finding all the four particles.

6.3.4. Dead Time

Trigger dead-time was about 2% per 10 KHz at L0 and about 0.2% per Hz at L2. Typical trigger rates were approximately 20 kHz at L0 and 25 Hz at L2. L1 had minimal dead-time. All these were accounted for in the determination of luminosity ($\mathcal{L}$). Any possible systematics were already incorporated in the uncertainty in $\mathcal{L}$.[25]

6.3.5. L0 Trigger Efficiency

The Monte Carlo did not simulate the tracking trigger at L0. In data taking, the tracking trigger lines at L0 typically required one (CLEO II) or two (CLEO II.V) hits in the barrel TOF counter and one charged track in VD. The requirement of 2 high P_T tracks in the good barrel in our event selection was specifically made to achieve high L0 trigger efficiency. The TOF was generally close to 100% efficient and VD was at least 85% efficient per track [26]. The distribution of events having

2, 3 and 4 tracks with high P_T ($>$ 225 MeV) in the good-barrel ($|\cos\theta|$ <0.71) was approximately 40%, 40% and 20% respectively. With this distribution of tracks, the probability of not having a single VD track, when there are 2, 3 and 4 tracks in the good-barrel can be calculated as below. We estimated the maximum inefficiency by assuming the non-barrel tracks would not produce a track in VD at all.

$$\begin{aligned}(1-\epsilon)_{max} \approx & \text{Prob(4 tracks in good barrel)} \times (0.15)^4 \\ & + \text{Prob(3 tracks in good barrel)} \times (0.15)^3 \\ & + \text{Prob(2 tracks in good barrel)} \times (0.15)^2 \qquad (29) \\ \Rightarrow (1-\epsilon)_{max} \approx & \ 20\% \times (0.15)^4 + 40\% \times (0.15)^3 + 40\% \times (0.15)^2 \approx 1\%\end{aligned}$$

We assigned 1% systematic uncertainty to our trigger efficiency due to L0 trigger. We did not make an explicit correction to the trigger efficiency, because the L0 trigger efficiency is more likely to be close to 100%, which Monte Carlo trigger simulation implicitly assumes by not simulating.

6.3.6. L1/L2 Trigger Efficiency

L1/L2 triggers were simulated in the Monte Carlo by a Monte-Carlo-Trigger-simulation (MCTR) package. However, various studies had shown that the tracking based L1 trigger efficiency as measured in data was lower than that predicted by the Monte Carlo. Brian Heltsley's study[27] of the tracking based trigger efficiency using $\tau^+\tau^- \rightarrow \rho^+\rho^-\nu_\tau\bar{\nu_\tau}$ events that satisfied the energy trigger had shown that the efficiency in data was 92%, 5% lower than the Monte-Carlo trigger simulation. Extrapolation of this discrepancy of 5% in 2 track events to our events having 4 tracks (tracks are similar in momentum) was done as follows:

Inefficiency for finding individual tracks in data was about 4%, a half of the inefficiency for finding 2 tracks (8%), whereas it was 1.5% in Monte Carlo. Note that our η_c events had in about 40% of cases 2 tracks in the good-barrel acceptances, 40% of cases 3 tracks in the good-barrel acceptances and 20% of cases 4 tracks in the good-barrel acceptances. The inefficiency for 2TRK L1/L2 trigger which typically required 2 TOF hits in the barrel, in addition to other VD and DR related information, can be calculated in the following way:

$$(1-\epsilon) \approx \text{Prob(4 tracks in good barrel and 3 didn't trigger)}$$
$$+\text{Prob(3 tracks in good barrel and 2 didn't trigger)}$$
$$+\text{Prob(2 tracks in good barrel and 1 didn't trigger)} \quad (30)$$

If the inefficiency was 4% as the τ data indicated, the net trigger inefficiency for the η_c events would be:

$$(1-\epsilon) \approx 20\% \times 4 \times (0.04)^3 + 40\% \times 3 \times (0.04)^2 + 40\% \times 2 \times (0.04) = 3.4\% \quad (31)$$

Repeating the above calculation, assuming the inefficiency for finding each track was 1.5%, resulted in an inefficiency of 1.2%. The discrepancy of 5% in the L1/L2 tracking based trigger efficiency in the 2 track $\tau^+\tau^-$ events between MC and data translated to a 2% discrepancy in the η_c events. This extrapolation corresponded to the worst case, when the tracks that were not in the good-barrel acceptances did not contribute at all to the trigger efficiency. Figure 10, shows that the distribution of the number of tracks within the barrel acceptances for η_c events and the number of events which were accepted by the Monte-Carlo trigger processor. It shows that even when only one track was in the barrel acceptance, 75% of the events satisfied the trigger requirements since many tracks in the endcap region also contribute to the trigger efficiency. A realistic estimate including the contribution of the tracks not in the good-barrel acceptances to the trigger efficiency yielded almost no discrepancy.

The same study by Heltsley showed that the Monte Carlo simulated efficiency of the TOF and CC components were in agreement with the corresponding efficiencies measured in data to within 1% accuracy per track. This implies that the 5% discrepancy was primarily due to non-TOF and non-CC components. We assigned 1% as our systematic uncertainty each for the TOF and CC component of the trigger. They were added in quadrature to obtain a combined systematic uncertainty of 1.5% for both CLEO II and CLEO II.V. A similar study by Urheim [28] in $\tau^+\tau^-$ decay to a lepton and a $\rho^\pm$, giving rise to 2 charged tracks in the final state, had estimated the L1/L2 tracking based trigger efficiency to be lower in data by about 1% compared to the Monte-Carlo prediction.

In addition to this, during the earlier part of CLEO II data sets (4s2 - 4s8 in CLEO data set designation) L2 trigger required that a track be found in the precision tracking device (PD) to satisfy the L2 trigger line. This requirement was found to

Table IX. Comparison of the trigger efficiencies in Monte Carlo and data.

Trigger	CLEO II MC (%)	CLEO II DATA (%)	CLEO II.V MC (%)	CLEO II.V DATA (%)
2TRK	91	91	96	96
BLTHAD	74	78	81	85
TSPHAD	52	65	69	79

have a systematic uncertainty of 2% [29] by comparing the Monte-Carlo predicted PD requirement efficiency with that measured in data. Averaging over the entire CLEO II data sets, this systematic uncertainty is reduced to 1% and added in quadrature to the rest of the L2 trigger efficiency uncertainty, resulting in a 2% systematic uncertainty for the CLEO II trigger efficiency.

As a consistency check, the trigger efficiency (L1/L2) of the 3 most efficient trigger lines that inclusively triggered all the selected η_c events were compared between Monte Carlo and data and are presented in Table IX. The efficiencies presented in this table are computed as the fraction of events satisfying a particular trigger line with respect to events having satisfied any trigger line used during the actual data taking.

6.3.7. L3 Trigger Efficiency

It is easier to estimate the systematic uncertainty due to the L3 trigger since it keeps every 8th event it would reject, unlike other triggers. So, one can look at the rejected events to find if any signal events were rejected and the reason for the rejection. After the analysis cuts, the L3 trigger efficiency estimated from the Monte Carlo was $\approx$ 95% in CLEO II and $\approx$ 91% in CLEO II.V. In data, we found two events each in CLEO II and CLEO II.V in the $K^0_S K^{\mp}\pi^{\pm}$ mass range near the η_c mass (2.8 - 3.15 GeV) that were tagged by L3 as rejected events. This means the L3 trigger must have rejected (14 $\pm$ 10) more events in CLEO II (out of a total of 14 + 435 = 449 events) and at least 14 more events in CLEO II.V (out of a total of 14 + 506 = 520 events), giving rise to L3 trigger efficiencies of $\approx$ 96% in CLEO II and $\approx$ 97% in CLEO II.V. The L3 trigger efficiency predicted by Monte Carlo agrees with data to within 1% in CLEO II, whereas there is a serious discrepancy in the L3 trigger efficiency predicted by Monte Carlo and data in CLEO II.V. We correct

the Monte Carlo predicted L3 trigger efficiency in CLEO II.V with the L3 trigger efficiency measured directly from the data.

Studying the events which would have been rejected in CLEO II, we found that one of the 2 events (Run number 65056, Event number 75694) actually came from a data set (4sE in CLEO data set designation scheme) when the VD was partially inoperative. Since the L3 trigger depended on hits in VD (2 hits out of first 5 layers and 3 hits out of 5 layers) and required 2 tracks in our case, it tagged the event as bad, because the K^0_S in this case conspired to decay outside the first five layers of VD. Monte Carlo did not take into account the inoperative VD and since this event should not have been rejected had VD been functioning properly and it possibly took away 7 more such events, which form $\approx 1\%$ of the total events in the signal window in CLEO II, we added this 1% in quadrature with the 1% difference between Monte Carlo and data L3 trigger efficiencies and assigned 1.5% systematic uncertainty to the L3 trigger efficiency of CLEO II. Due to the difference in the Monte Carlo predicted L3 trigger efficiency and that from data in CLEO II.V, we assigned a systematic uncertainty of 3% to the CLEO II.V L3 trigger efficiency.

6.3.8. K^0_S finding Efficiency

Studies using $\tau^- \to K^{*-}(892)\nu_\tau$ decay, where the $K^{*-}(892)$ decays to $K^0_S\pi^-$, by Urheim [30] had shown that the K^0_S finding efficiency modeled in Monte Carlo was good to 1% level in both CLEO II and CLEO II.V. The $K^{*-}(892)$ which subsequently decayed to a K^0_S and a π^- was an ideal choice for the study of the reconstruction efficiency of the K^0_S, since the large width of the $K^{*-}(892)$ (≈ 51 MeV) allowed for even poorly reconstructed K^0_S to produce a reconstructed $K^{*-}(892)$, thus enabling the study of K^0_S finding efficiency. Our K^0_S momentum distribution and selection criteria for the K^0_S were similar to this study done by Urhiem. We assigned a 1% systematic uncertainty to the K^0_S finding efficiency.

6.3.9. Resonant Sub-structure in the η_c decay

The η_c meson may decay to $K^*\bar{K}$ before it decays to the $K^0_S K^\mp \pi^\pm$ final state. If the fraction of this contribution is large, the efficiency for detecting η_c decays may be different from our estimate, which assumes 3-body phase-space decays of the η_c.

We generated $\eta_c \to K^*\bar{K} \to K^0_S K^\mp \pi^\pm$ Monte Carlo and obtained their detection efficiency. The efficiency for $K^*\bar{K}$ decay differs from the phase space decay by at most 2%. Even if half of these η_c decays proceed through $K^*\bar{K}$, the systematic uncertainty is 1%. We assigned a 1% systematic uncertainty to the efficiency due to possible presence of $K^*\bar{K}$ resonant sub-structure in the η_c decay to the final state $K^0_S K^\pm \pi^\mp$. See Appendix B for detailed descriptions.

6.3.10. Feed-down from Higher Resonances

The higher resonances produced in two-photon processes that can feed down to η_c via decays to the J/ψ and subsequent radiative decay of the J/ψ to the η_c are the χ_{c0} and χ_{c2} mesons. These feed-downs can be estimated by taking the ratio of the cross section of the higher resonance to the cross-section of η_c and then multiplying the number of η_c events observed with the product branching fractions corresponding to the decay of the higher resonance to J/ψ and J/ψ to η_c. The expected number of events were corrected for the corresponding two-photon partial widths. The estimated feed down to η_c from χ_{c0} and χ_{c2} are 0.0 and 0.5 events, respectively.

We also estimated the feed-downs from J/ψ produced in the process $e^+e^- \to \gamma(J/\psi)$. The J/ψ produced via this process has a large momentum of around 4.9 GeV, which means the η_c produced from the radiative decay of this J/ψ would also be at a very high momentum since the η_c would be almost collinear with this J/ψ and carry most of the momentum. An explicit momentum cut of 4.5 GeV on the η_c candidate was applied to determine if there was any η_c coming from the radiative decay of the J/ψ via the above process. We did not find any such candidate. The momentum of the η_c produced in such radiative process is higher than the maximum possible momentum for the η_c produced in the two-photon process and at such high momentum the daughter tracks would be highly boosted towards the endcap (since that is the predominant direction of emission of the radiatively produced J/ψ). Such events have low 2TRK trigger efficiency. The expected number of such η_c candidates from radiative J/ψ decays are consistent with zero.

We did not assign any systematics uncertainty to the η_c yield due to possible feed-down from higher resonances produced in the two-photon process.

Table X. Effect of particle mis-identification on the efficiency estimate of the 3σ consistency requirement.

Particle	CLEO II MC ϵ	CLEO II DATA ϵ	CLEO II.V MC ϵ	CLEO II.V DATA ϵ
$\pi_{highmom}$	96.4%	96.5%	96.3%	97.2%
π_{lowmom}	92.3%	93.2%	93.2%	94.1%

6.3.11. Detector Resolution

Since we did not fix the width of the η_c from Monte Carlo generated with an assumed Breit-Wigner width, we were not affected by any small uncertainties in the detector resolution, beyond what had already been included in the statistical uncertainty. We did not assign any systematic uncertainty to the efficiency due to possible uncertainties in the detector resolution.

6.3.12. Particle ID

To keep the uncertainties in the particle identification procedure low we used it only on one track in the event - the charged kaon or charged pion depending on the one that had the lower momentum and applied a loose 3σ dE/dx consistency cut. We checked the efficiency of the 3σ cut using a reasonably pure sample of pions selected from the decay of K^0_S. The $\delta_{E_{\rm loss}}$, which is the difference between the measured and expected dE/dx normalized to the dE/dx resolution, distribution of high momentum pions (typically 700 MeV) and low momentum pions (typically 300 MeV) in Monte Carlo were compared with those from the data. The distributions showing the comparison between Monte Carlo and data can be seen in Figure 26 and Figure 27 for CLEO II and CLEO II.V, respectively. The efficiency of a 3 σ cut in Monte Carlo and data are compared in Table X for both CLEO II and CLEO II.V. There is a discrepancy of up to 1% in the efficiency of the 3 σ cut between Monte Carlo and data. This discrepancy was found to arise from the Monte Carlo modeling of the number of dE/dx measurements for tracks.

Alternatively, we compared the change in the K^0_S yield in Monte Carlo and data, when we required a 3σ consistency for the daughter pions. We did this comparison by performing a fit to the K^0_S invariant mass distribution using a double Gaussian for

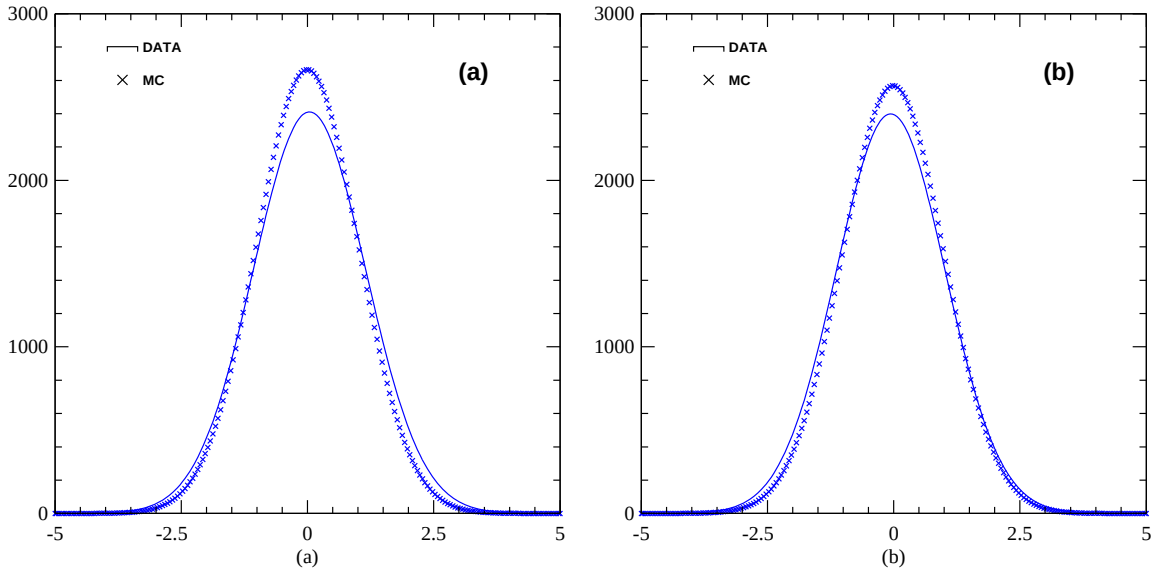

Fig. 26. $\delta_{E_{\rm loss}}$ distributions in MC and data, for the (a) higher momentum pions and (b) lower momentum pions from K^0_S in CLEO II.

Table XI. Effect of particle mis-identification on the efficiency estimate in the K^0_S yield

Particle	II MC ϵ	II DATA ϵ	II.V MC ϵ	II.V DATA ϵ
$\sigma_{highmom} < 3$	96.7%	98.5%	96.1%	98.4%
$\sigma_{lowmom} < 3$	93.3%	94.3%	93.2%	95.0%

the signal and 2nd order Chebysev Polynomial for the background. The results are summarized in Table XI.

We found that the K^0_S yield in both CLEO II and CLEO II.V was consistent between Monte Carlo prediction and data within 2% for the results obtained from performing a fit, which properly handled the K^0_S's reconstructed out of random particles.

Similar to the procedure adopted in the Section 6.2.2 to estimate the effect of the uncertainty in the particle identification procedure on the fraction of mis-identified events, we completely removed and doubled the fraction of mis-identified events in the Monte Carlo sample to obtain the fit parameters. We then used these fit parameters to perform the fit on the mass distribution obtained from data. The maximum change in yield was 1.5% in both CLEO II and CLEO II.V.

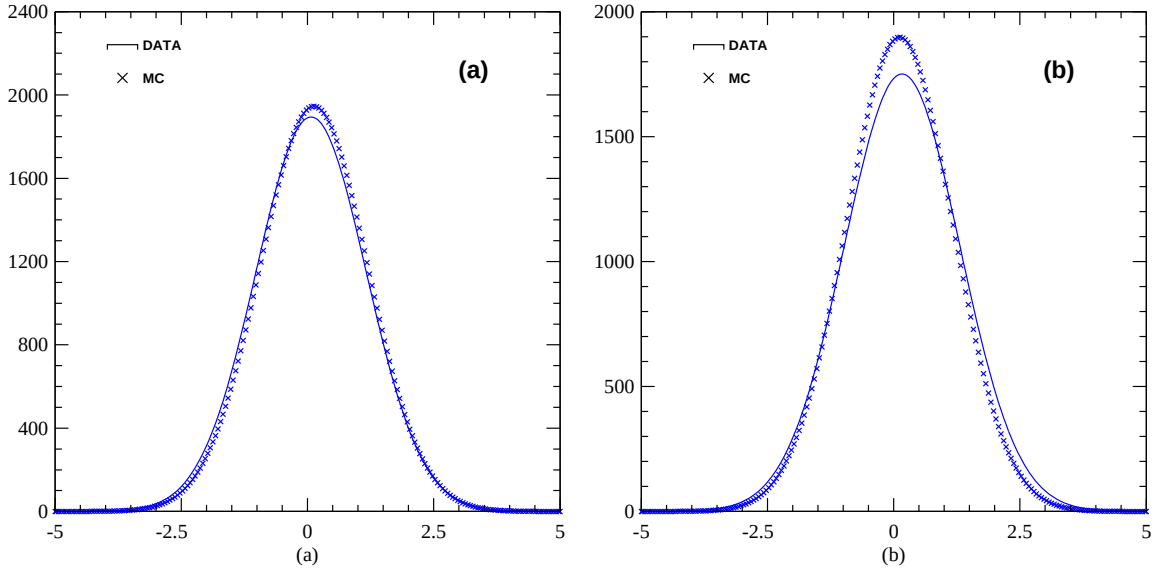

Fig. 27. $\delta_{E_{\rm loss}}$ distributions in MC and data, for the (a) higher momentum pions and (b) lower momentum pions from K^0_S in CLEO II.V.

We assigned the higher 2% systematic uncertainty arising out of the 3σ consistency requirement, due to possible uncertainties in the particle identification procedure in both CLEO II and CLEO II.V.

6.3.13. Background Function

Similar to reasons discussed in Section 6.1.3, we did not assign any additional systematic uncertainty to the measured two-photon partial width of the η_c due to possible uncertainties in the shape of the background.

6.3.14. Signal Shape Parameters

The three parameters that are used in the fit to the invariant mass distribution in data (which gives the yield) were obtained from the "$\Gamma^{\eta_c}_{tot} = 0$ MeV" Monte Carlo. The effect of variation in the width of the narrower Gaussian on the yield in data has already been accounted for as part of the statistical uncertainty in the fit. We varied the other two parameters in the fit to the invariant mass distribution in data by $\pm$ 15%, similar to what has been described in Sections 6.1.4 and 6.2.4, and studied

Table XII. Effect of signal-shape variation on the η_c yield in data.

Shape Parameter	Total Yield (II)	$\Gamma^{\eta_c}_{\gamma\gamma}$(II)	Total Yield (II.V)	$\Gamma^{\eta_c}_{\gamma\gamma}$(II.V)
Nominal	130	7.6	168	7.5
σ_2/σ_1 +15%	131	7.6	169	7.5
σ_2/σ_1 -15%	129	7.5	167	7.4
A_2/A_1 +15%	130	7.6	168	7.5
A_2/A_1 -15%	129	7.5	168	7.5

the effects on η_c yield. The result of the variation of the signal shape parameters are summarized in Table XII.

The measured $\Gamma^{\eta_c}_{\gamma\gamma}$ changed by up to 1% due to the variation in σ_2/σ_1 in both CLEO II and CLEO II.V and changed by up to 1% due to the change in A_2/A_1 in CLEO II and up to 0.2% in CLEO II.V. We added these two systematic uncertainties in quadrature and assigned a 1.5% systematic uncertainty for CLEO II and a 1% systematic uncertainty for CLEO II.V partial width measurements due to possible uncertainties in the signal shape parameters.

6.3.15. Interference

Similar to the reason why we ignore the effect of interference on the measured mass, we ignore any possible effect of interference on the measured two-photon partial width. We do not assign any systematic uncertainty to the measured two-photon partial width of the η_c due to possible interference effects.

6.3.16. Consistency Check

As a consistency check, we studied the two decay modes $\eta_c \to K^0_S K^-\pi^+$ and $\eta_c \to \overline{K}^0_S K^+\pi^-$ separately. We obtained consistent number of events in both decay modes, (163 $\pm$ 22) events in the $\eta_c \to K^0_S K^-\pi^+$ decay and (138 $\pm$ 21) events in the $\eta_c \to \overline{K}^0_S K^+\pi^-$ decay - in the combined data sets. We also studied any possible discrepancy in the yield in the forward/ backward directions. The η_c yields were

consistent within uncertainties (153 ± 22) events in the positron direction and (144 ± 22) events in the electron direction. The CLEO II and CLEO II.V yields were consistent with each other after efficiency and luminosity were taken into account.

6.3.17. Branching Fraction

The branching fraction $\mathcal{B}(\eta_c \to K\bar{K}\pi)$ quoted by the PDG (5.5 ± 1.7)% has a ±30% uncertainty which consists of the error in the radiative branching fraction $\mathcal{B}(J/\psi \to \gamma\eta_c)$ measurement from the Crystal Ball experiment [8] and the error in the product branching fraction $\mathcal{B}(J/\psi \to \gamma\eta_c) \times \mathcal{B}(\eta_c \to K\bar{K}\pi)$ from DM2 [31] and MARK III [32] experiments. This is common to all experiments which use the $\eta_c \to K\bar{K}\pi$ decay mode. We present the uncertainty due to the branching fraction as a separate source of systematic uncertainty to the $\Gamma^{\eta_c}_{\gamma\gamma}$ measurement since in the future the branching fraction uncertainty may go down with better measurements and one can change our result and that portion of the systematic uncertainty in our result appropriately. We assigned the full 30% uncertainty in the branching fraction to the systematic uncertainty on $\Gamma^{\eta_c}_{\gamma\gamma}$.

PDG lists the error on $\Gamma^{\eta_c}_{\gamma\gamma}$ to be 20%. Given the fact that the branching fraction systematic is common to all experiments, this small overall systematic uncertainty is mysterious. Note that even $\Gamma^{\eta_c}_{\gamma\gamma}$ measurements made using η_c decay modes other than $K\bar{K}\pi$ decay mode share at least $\mathcal{B}(J/\Psi \to \gamma\eta_c)$ uncertainty and their errors due to $\mathcal{B}(J/\Psi \to \gamma\eta_c) \times \mathcal{B}(\eta_c \to$ modes of interest) is substantially larger than that for the $K\bar{K}\pi$ decay mode.

7. SUMMARY

We have measured the mass, total decay width and two-photon partial width of the η_c meson produced in two-photon collisions. The systematic uncertainty in M_{η_c} was dominated by the uncertainty in the mass calibration of our detector. The final mass measurement of (2980.4 ± 2.3 (stat) ± 0.6 (syst)) MeV compares well with the world average of (2979.8 ± 2.1) MeV [4].

The result for the total decay width is (27.0 ± 5.8 (stat) ± 1.6 (syst)) MeV and it disagrees with the 1998 world average of (13.2 ± 3.5) MeV [4] at the 2σ level. However, most of the width measurements going into that average had large

individual relative errors and differed from each other substantially. The various width measurements published so far including recent results from E835 [33] and BES [34] are shown in Figure 28 along with our result [37]. The PDG averages the various width measurements using the standard error-weighted averaging method. However, we feel that a logarthimic average of the various measurements, where the fractional errors instead of simple errors matter, would be a more appropriate indicator of the world average. The total width measurement is dominated by the measurements from E835 and CBAL. Taking a simple error weighted average of these two measurements gives an average of (13.6 ± 4.1) MeV, whereas their logarthimic average is (16.2 ± 4.6) MeV.

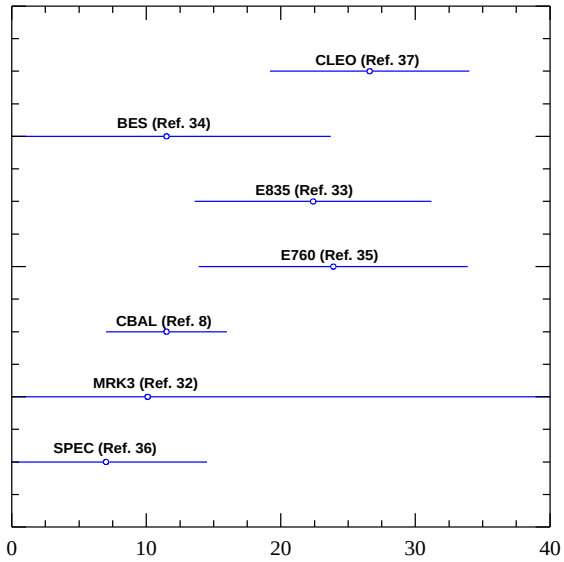

Fig. 28. η_c Width Measurements (MeV) from Various Experiments.

The measured two-photon partial width of the η_c meson of (7.6 ± 0.8 (stat) ± 0.4 (syst)) keV agrees well with the world average [4] of (7.5 ± 1.5) keV and theoretically expected values, and is a significant improvement in terms of experimental precision. We use the world average[4] of the $\eta_c \to K\overline{K}\pi$ branching fraction of (5.5 ± 1.7)%. The uncertainty in $\Gamma^{\eta_c}_{\gamma\gamma}$ due to the uncertainty in this branching fraction is ±2.3 keV and is stated separately from the other contributions.

From the ratio of our measured total width and two-photon partial width, we calculated the value of the strong coupling constant at the charm mass scale as 0.285 ± 0.025. This calculated value evolved to the Z-scale gives a value of $\alpha_s(Z) = 0.117 \pm 0.010$, which compares well with the world average value at Z-scale of 0.116

$\pm$ 0.003 [4]. The value of α_s at the charm mass scale was obtained using the NLO perturbative calculation given in Equation 6, thus making the result renormalization scheme and renormalization scale dependent.

Our measurements of $\Gamma^{\eta_c}_{\rm tot}$ and $\Gamma^{\eta_c}_{\gamma\gamma}$ show that PQCD calculations are able to reliably predict the ratios of the decay rates of a heavy quarkonium system, where non-perturbative effects cancel.

Appendix A

Two-photon Physics and the Helicity Basis

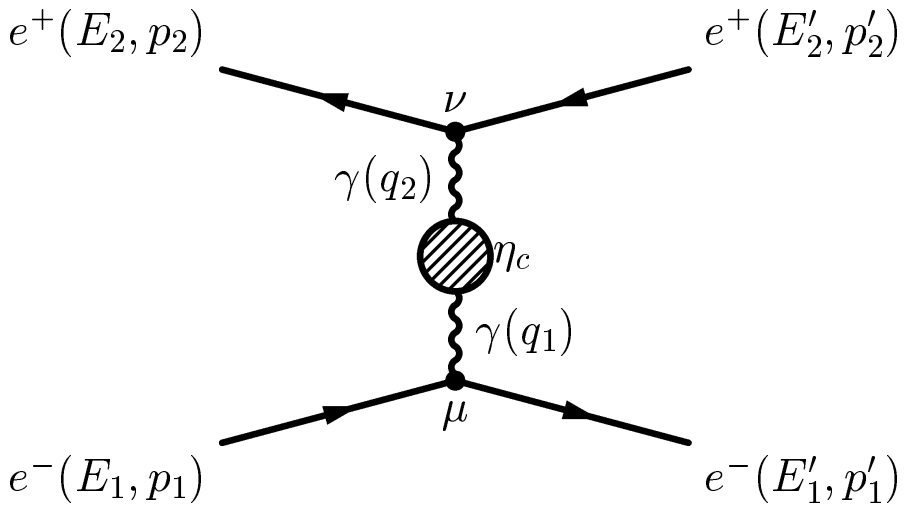

Fig. A.1. $\gamma\gamma$ production of η_c.

The cross-section for the complete quantum mechanical description of the two-photon production of a resonance, as shown in Figure A.1 has been given by V. M. Budnev *et al* [13] and others. For unpolarized electron beams,

$$d\sigma = \frac{\alpha^2}{16\pi^4 q_1^2 q_2^2}\sqrt{\frac{(q_1q_2)^2 - q_1^2q_2^2}{(p_1p_2)^2 - m_1^2m_2^2}}\{4\rho_1^{++}\rho_2^{++}\sigma_{TT} + 2|\rho_1^{+-}\rho_2^{+-}|\tau_{TT}\cos(2\phi)$$

$$+2\rho_1^{++}\rho_2^{00}\sigma_{TL} + 2\rho_1^{00}\rho_2^{++}\sigma_{LT} + \rho_1^{00}\rho_2^{00}\sigma_{LL} - 8|\rho_1^{+0}\rho_2^{+0}|\tau_{TL}\cos(\phi)\}\frac{d^3p_1'}{E_1'}\frac{d^3p_2'}{E_2'}, \quad \text{(A.1)}$$

The labels +, -, 0 refer to the helicities of the photons in the $\gamma\gamma$ center of mass system. The angle ϕ is the angle between the electron-γ planes in the $\gamma\gamma$ center of mass system. The flux factors are given by

$$2\rho_1^{++} = 2\rho_1^{--} = \frac{1}{X}(2p_1q_2 - q_1q_2)^2 + 1 + \frac{4m_e^2}{q_1^2} \quad \text{(A.2)}$$

$$\rho_1^{00} = \frac{1}{X}(2p_1q_2 - q_1q_2)^2 - 1 \tag{A.3}$$

$$|\rho_1^{+0}\rho_2^{+0}|\cos(\phi) = \frac{4}{X}(2p_1q_2 - q_1q_2)(2p_2q_1 - q_1q_2)C\frac{1}{\sqrt{q_1^2q_2^2}} \tag{A.4}$$

$$2|\rho_1^{+-}\rho_2^{+-}\cos(2\phi) = \frac{C^2}{q_1^2q_2^2} - 2(\rho_1^{++} - 1)(\rho_2^{++} - 1) \tag{A.5}$$

$$|\rho_i^{+-}| = \rho_i^{++} - 1 \tag{A.6}$$

$$|\rho_2^{a,b}(1,2)| = |\rho_1^{a,b}(2,1)| \tag{A.7}$$

where,

$$= (2p_1 - q_1)(2p_2 - q_2) + \frac{1}{X}(2p_1q_2 - q_1q_2)(2p_2q_1 - q_1q_2), \tag{A.8}$$

and $X = (q_1q_2)^2 - q_1^2q_2^2$. In the virtual photon center of mass system, $X/W_{\gamma\gamma}^2$ is the squared three-momentum of a photon.

The suffixes T and L for the cross section terms σ and τ stand for combinations of transverse and longitudinal photon contribution to the total cross section; so σ_{TT} corresponds to the cross-section term for a transverse photon interacting with a transverse photon. The τ terms represent the interfering cross-section terms; τ_{TT} represents the difference between cross-sections for scattering transverse photons with the parallel ($\sigma_\parallel$) and orthogonal ($\sigma_\perp$) linear polarizations. So, $\tau_{TT} = \sigma_\parallel$ - $\sigma_\perp$, whereas $\sigma_{TT} = (\sigma_\parallel + \sigma_\perp)/2$.

We can express the cross-sections in the helicity basis by relating the absorptive part of the forward $\gamma\gamma$-scattering amplitude $W_{a'b',ab}$ with the amplitudes M_{ab} for the $\gamma\gamma \to$ hadrons as follows

$$W_{a'b',ab} = \frac{1}{2}\int M_{a'b'}^* M_{ab}(2\pi)^4\delta^4(q_1 + q_2 - \Sigma_i k_i)d\Gamma = T_{\mu\nu}\epsilon_{1a}^\mu\epsilon_{2b}^\nu, \tag{A.9}$$

where, $d\Gamma = \prod_i \frac{d^3k_i}{2E_i(2\pi)^3}$ is the product phase space for the final states. Now, the various cross-section terms are

$$2\sqrt{X}\sigma_{TT} = W_{TT} = \frac{1}{2}(W_{++,++} + W_{--,--}) \tag{A.10}$$

$$2\sqrt{X}\sigma_{TL} = W_{TL} = W_{+0,+0} \tag{A.11}$$

$$2\sqrt{X}\sigma_{LT} = W_{LT} = W_{0+,0+} \tag{A.12}$$

$$2\sqrt{X}\sigma_{LL} = W_{LL} = W_{00,00} \tag{A.13}$$

$$2\sqrt{X}\tau_{TT} = W^{\tau}_{TT} = W_{++,--} \tag{A.14}$$

$$2\sqrt{X}\tau_{TL} = W^{\tau}_{TL} = \frac{1}{2}(W_{++,00} + W_{0+,-0}) \tag{A.15}$$

The two-photon vertex $T_{\mu\nu}$ is subject to a number of conservation laws, in particular, charge conjugation invariance, gauge invariance, Lorentz invariance, angular momentum conservation, Bose statistics and conservation of parity. The charge conjugation invariance implies, only even charge conjugation states can be produced in a $\gamma\gamma$ process (since photon has negative C-parity). Additionally, it also implies that the photon fusion mechanism is the only second order QED $e^+e^- \to e^+e^-X$ amplitude in which the final state X is linked to the leptonic system via two photons. All other second order QED diagrams (Bremsstrahlung, annihilation and conversion) thus describe formation of states with negative charge conjugation. The consequences of other symmetry principles are summarized below. For state of specific spin parity J^P, the helicity matrix elements $M_{a,b}$ are

$$M_{0,b}(q_1^2, q_2^2) \sim \sqrt{-q_1^2} \;\; (\text{as } q_1^2 \to 0) \quad \text{for all} \;\; J^P \quad \text{gauge invariance} \tag{A.16}$$

$$M_{a,0}(q_1^2, q_2^2) \sim \sqrt{-q_2^2} \;\; (\text{as } q_2^2 \to 0) \quad \text{for all} \;\; J^P \quad \text{gauge invariance} \tag{A.17}$$

$$M_{a,b}(q_1^2, q_2^2) = M_{-a,-b}(q_1^2, q_2^2) \quad \text{for} \;\; J^P = 0^+, 1^-, 2+, \ldots \quad \text{parity} \tag{A.18}$$

$$M_{a,b}(q_1^2, q_2^2) = -M_{-a,-b}(q_1^2, q_2^2) \quad \text{for} \;\; J^P = 0^-, 1^+, 2-, \ldots \quad \text{parity} \tag{A.19}$$

$$M_{a,b}(q_1^2, q_2^2) = (-1)^{(J-a+b)} M_{b,a}(q_2^2, q_1^2) \quad \text{for all} \;\; J^P \quad \text{Bose symmetry} \tag{A.20}$$

$$M_{a,b}(q_1^2, q_2^2) = \delta^J_{(a-b)} M_{a,b}(q_1^2, q_2^2) \quad \text{with} \;\; J_z \leq J \quad \text{Lorentz invariance} \tag{A.21}$$

These conservation laws restrict the helicities of the hadron produced by the two-photon fusion mechanism, for various q^2 values and various tagged conditions.

For quasi-real photons ($q_1^2 = q_2^2 \to 0$), the restrictions are most severe. In this case, all selection rules stated above apply, and only a small number of amplitudes remains non-zero

$$M_{\pm,\pm}(J^P = 0^\pm, 2^\pm, 4^\pm, \ldots) \neq 0 \tag{A.22}$$

$$M_{\pm,\mp}(J^P = 2^+, 3^+, 4^+, \ldots) \neq 0 \tag{A.23}$$

$$\text{all others vanish} \tag{A.24}$$

These amplitude restrictions imply Yang's theorems:

$$\sigma(1^+) = \sigma(1^-) = 0 \tag{A.25}$$

$$\sigma(J^P = 3^-, 5^-, 7^-, \ldots) = 0 \tag{A.26}$$

and fix for a large number of states, with which helicities they are produced in the collisions of almost real photons. Therefore, in most of the cases, the helicities are fixed by first principles.

Since, η_c is a pseudo-scalar (0^-) meson, as explained above, it can only have $M_{\pm,\pm}$ non-zero matrix elements, which means, it can only have σ_{TT} and τ_{TT} cross-section terms. Additionally, amplitudes connecting two photons with a state of "abnormal" parity ($J^P = 0^-, 1^+, 2^-, \ldots$) must contain the anti-symmetric tensor once[12]. Using these two facts along with the fact that η_c is a neutral meson, one concludes that $\gamma\gamma$ coupling to η_c has only one form factor.

$$T_{\mu\nu} = i\epsilon_{\mu\nu\alpha\beta} q_1^\alpha q_2^\beta F(q_1^2, q_2^2) \tag{A.27}$$

The only non-zero amplitudes $M_{\pm,\pm}$ imply that the η_c can not couple to longitudinally polarized photons; it only couples to transversely polarized photons.

Appendix B

Resonant Sub-structure in η_c Decay

One of the long-standing issues regarding the decay of η_c to $K^0_S K^{\pm}\pi^{\mp}$ has been whether there is a resonance sub-structure in the η_c decay in the form of $K^*(1430)\bar{K}$. Without knowing what fraction of contribution comes from this $K^*\bar{K}$ decay to the final state of $K^0_S K^{\pm}\pi^{\mp}$, it is difficult to do the two-photon partial width calculation. A simple 3 body phase space decay may not be a good enough description. The matrix element of the decay

$$\eta_c \to K^*\bar{K} \to (K\pi)\bar{K} \tag{B.1}$$

involves two L=2 couplings. Since the K^* is an isospinor, the $K^{\pm}K^0\pi^{\mp}$ can proceed either through a charged or a neutral K^*. For example:

$$M(\eta_c \to K^+K^0\pi^-) = M(\eta_c \to (K^{*0} \to K^+\pi^-)K^0) + M(\eta_c \to (K^{*-} \to K^0\pi^-)K^+) \tag{B.2}$$

and the amplitudes are equal in magnitude. Though in our analysis, the fact that the $K\bar{K}\pi$ final state was detected far above the threshold and hence the final result was quite independent of the assumed decay dynamics, having such a large sample of η_c events, we were in an unique position to shed light on this issue. We looked for presence of $K^*\bar{K}$ in the decay of η_c candidates.

To obtain the number of events of the type $\eta_c \to K^*\bar{K}$, we fit to the invariant mass distribution of the η_c candidates in bins of both the charged $K^{*\pm}$ ($K^0_S\pi^{\pm}$) and neutral K^{*0} ($K^{\mp}\pi^{\pm}$) invariant masses. Then the η_c yield was plotted versus the corresponding K^* masses as shown in Figure B.1. Figure B.1 shows the fits to the $K^*_2(1430)$ as well $K^*(892)$ (charged and neutral) for K^* events consistent with coming from a η_c decay, by obtaining the yield of η_c in bins of K^* mass, in the combined CLEO II and CLEO II.V data sets. We ignored the other nearby, very wide resonances like $K^*_0(1430)$, $K^*(1680)$ and their interference due to decay to the same final states as the states under study and treated them as non-resonant background events.

We found a contribution of 73 $\pm$ 15 events from the $K^{*\pm}_2(1430)K^0$ decay mode and 62 $\pm$ 15 events from the $K^{*0}_2(1430)K^{\mp}$ decay mode in the combined data sets.

Together, they formed approximately $(45 \pm 10)\%$ of the total η_c events (≈ 300 events). To estimate the effect of having such a decay on the two-photon partial width, we did an estimate of the detection efficiency of such a decay mode and found that it was at most different from the detection efficiency of the 3 body $K^0_S K^{\pm}\pi^{\mp}$ decay mode by 2%. So, even if half the decay were to proceed via the $K^*_2(1430)\bar{K}$, the effective efficiency would be off by about 1%. We assigned the whole 1% as systematic uncertainty due to the possible $K^*_2(1430)\bar{K}$ resonance sub-structure in the η_c decay to the final states of our interest. One should note that, the number of events for the $K^{*0}_2(1430)K^0$ and $K^{*\pm}_2(1430)K^{\mp}$ decays of η_c were obtained by fixing the mass and width of the $K^*(892)$ and $K^*_2(1430)$ at the PDG values. The fraction of events where η_c decayed through $K^*(892)\bar{K}$ as obtained from the fits was consistent with zero, both in the charged and neutral $K^*(892)$ channels.

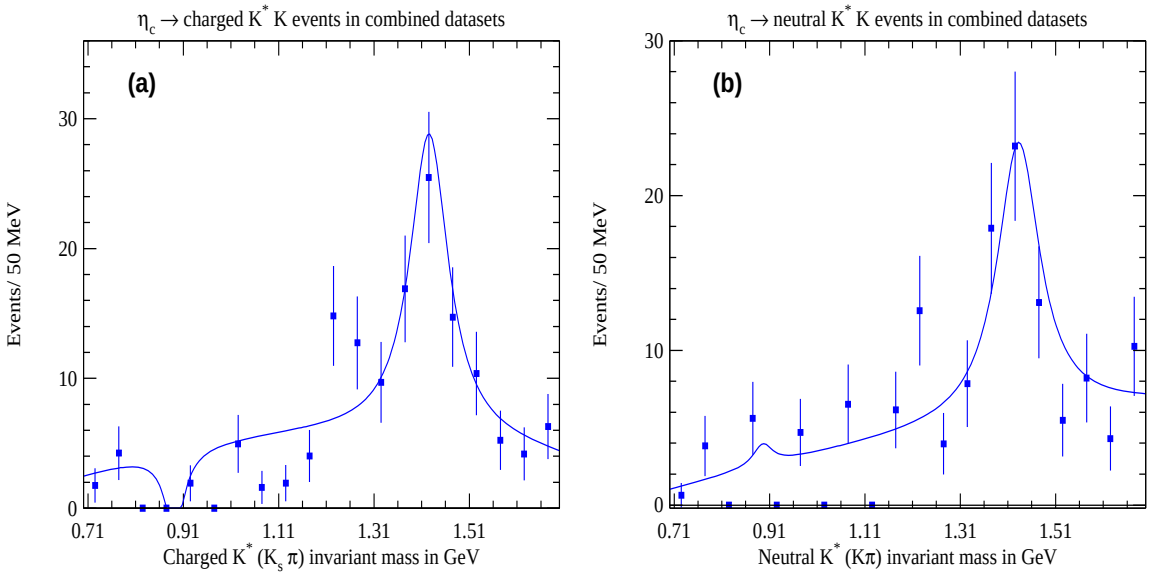

Fig. B.1. Fit to $K^{*\pm}_2(1430)$ and $K^{*\pm}(892)$ obtained from the fits to η_c in bins of K^* mass, for (a) charged K^* and (b) neutral K^*.

Appendix C

Monte Carlo Generation

The two-photon production of the η_c resonance was characterized by five independent variables; the relative azimuthal angle of the scattered electrons (ϕ), their two polar angles (θ_1, θ_2), the energy of one of the photons (ω_1) and the center of mass energy of the two photons (W).

To generate a single event each independent variable was assigned a particular value from a set of possible values according to the probability density function (p.d.f.) for that variable. The p.d.f. $p(x)$, for a random variable x was defined so that the probability of observing x between $x + dx$ is $p(x)dx$.

For each variable, the Monte Carlo generator started with a random number (periodicity more than 10^{13}) from a uniform distribution on the interval (0,1). This random number was mapped into the independent variable producing a set o f random numbers with the desired range and distribution. This mapping was done using a technique called importance sampling.

The concept of importance sampling is to generate points (i.e. particle four-momenta) not uniformly, but in a "compressed" space, where the integrand (i.e. differential cross-section) has maxima.

We obtained the cross-section for the process $e^+e^- \to e^+e^-\gamma\gamma \to e^+e^-\eta_c$ by doing a numerical integration of the differential cross-section as given in Eq. 9, from the formalism of Budnev *et al* [13]. In the multi-dimensional space of five independent variables, we defined a product vector space and the integration volume was the product of individual differential elements of those variables.

The line shape of the η_c meson was modeled by a Breit-Wigner distribution with total width $\Gamma_{tot}^{\eta_c}$. Starting with a random number x, uniform on (0,1), we generated the W distribution according to,

$$W = M_{\eta_c} + \frac{\Gamma_{tot}^{\eta_c}}{2} \tan[(2x-1)\pi/2] \tag{C.1}$$

For the other variables we used the importance sampling method. The relative azimuthal angle of the scattered electrons ϕ was generated uniformly on the interval

$(0,2\pi)$ as, $\phi = 2\pi u$. So, the normalized envelope function was then $p_\phi(\phi) = 1/2\pi$. The electron scattering angle, θ, is sharply peaked towards zero. To generate θ values, we used an envelope function proportional to $1/\theta$. The photon energy ω is also sharply peaked towards zero and we similarly used an envelope function of the form $1/\omega$.

After the generation of the events, they were propagated through the detector elements by a detector simulation package (CLEOG), based upon GEANT [38], which simulated the response of the various detector elements. Finally, the raw events were processed by a reconstruction package (PASS2), which reconstructed the four-momenta of all the tracks in the event, neutral energy deposits in the calorimeter along with a host of other event variables.

Appendix D

Radiative Decay Rates between Charmonium States

Non-relativistic estimate for the partial width of the $J/\psi \to \gamma\eta_c$ has been given as [9]

$$\Gamma(J/\psi \to \gamma\eta_c) = \frac{2}{9}\frac{\Gamma(\eta_c \to \gamma\gamma)}{\Gamma(J/\psi \to e^+e^-)} \times \alpha\frac{m_{J/\psi}^4}{m_{\eta_c}^3} \times (1 - m_{\eta_c}^2/m_{J/\psi}^2)^3 \times (1 + O(\alpha_s)). \tag{D.1}$$

Using the world average value of $\Gamma(\eta_c \to \gamma\gamma)$ as (7.5 ± 1.5) keV [4] and that of $\Gamma(J/\psi \to e^+e^-)$ as (5.3 ± 0.4) keV [4], the estimated partial width of $\Gamma(J/\psi \to \gamma\eta_c)$ is (3.3 ± 0.7) keV. The Crystal Ball collaboration first measured this partial width in 1980 as (1.1 ± 0.4) keV [39].

This discrepancy in the branching fraction (partial width) for the radiative decay of J/ψ to η_c had been a source of controversy for some years in the early 80's. Experimentally this branching fraction $\mathcal{B}(J/\psi \to \gamma\eta_c)$ is an important input to measurements of the η_c decay branching fractions, since they are measured from the radiative decay of J/ψ to $\gamma\eta_c$ followed by subsequent decay of η_c to final states. Uncertainty or incorrectness of the $\mathcal{B}(J/\psi \to \gamma\eta_c)$ measurement directly affects the $\mathcal{B}(\eta_c \to \text{hadrons})$.

Due to this discrepancy between the non-relativistic PQCD prediction and experimentally measured $\mathcal{B}(J/\psi \to \gamma\eta_c)$ and its importance in the deduction of $\mathcal{B}(\eta_c \to \text{hadrons})$, the Crystal Ball collaboration reanalyzed the $\mathcal{B}(J/\psi \to \gamma\eta_c)$ measurement with twice the number of J/ψ mesons (2.2 million) and published their result in 1986 [8]. This measurement resulted in a value for the $\mathcal{B}(J/\psi \to \gamma\eta_c)$ of $(1.27 \pm 0.36)\%$, which was still 3 times lower than the theoretically predicted branching fraction of 3.8%.

Subsequently, measurements were made for the partial widths of various radiative transition between charmonium systems, namely between the ψ' and χ_c states as well as between the χ_c states and the J/ψ. It was found out that the non-relativistic PQCD predictions for all these radiative partial widths were higher than the experimentally measured values. The discrepancies between the non-relativistic PQCD

Table D1: Comparison between non-relativistic PQCD predictions [2] and experimentally measured radiative partial widths [4]

Radiative transition	NR PQCD prediction (keV)	Experimental result (keV)
$J/\psi \to \eta_c$	3.3	1.1
$\psi' \to \chi_{c0}$	38	26
$\psi' \to \chi_{c1}$	34	24
$\psi' \to \chi_{c2}$	30	22
$\chi_{c0} \to J/\psi$	155	89
$\chi_{c1} \to J/\psi$	320	240
$\chi_{c2} \to J/\psi$	355	270

predictions and experimental results for the radiative $E1$ transitions between the charmonium states however are not very large with only up to 75% discrepancy. The $E1$ transition involves states of different parity and hence different wave-functions. Taking into account that there is more dependence on the meson wave-function in the calculation of the $E1$ transition rate, the discrepancy between the non-relativistic PQCD predictions and experimental results is not very serious due to the higher theoretical uncertainties involved in such calculations. On the other hand, for the $M1$ transition between the J/ψ and the η_c, the wave functions are expected to be more similar and hence the discrepancy between the non-relativistic PQCD prediction and experimental result is puzzling.

A summary of the theoretical predictions [2] and the experimentally measured values is given in Table D1.

References

1. D. J. Gross and F. Wilczek, "Asymptotically Free Gauge Theories. I.", Physical Review **D8** (1973) 3633.
2. V. A. Novikov *et al*, "Charmonium and Gluons", Physics Reports **C41** (1978) 1.
3. Y. Chen and R. J. Oakes, "The Hyperfine Spin Splittings in Heavy Quarkonia", LANL electronic publishing archive hep-ph/9506377, 1995.
4. Particle Data Group, "Review of Particle Physics", The European Physics Journal **C** (1998).
5. G. P. Lepage and S. J. Brodsky, "Exclusive Processes in Perturbative QCD", Physical Review **D22** (1980) 2157.
6. W. Kwong *et al*, "Quarkonium Annihilation Rates", Physical Review **D37** (1988) 3210.
7. K. Chao *et al*, "Pseuduscalar Heavy Quarkonium Decays With Both Relativistic and QCD Radiative Corrections", LANL electronic publishing archive hep-ph/9601381, 1996.
8. R. Gaiser *et al.*, "Charmonium Spectroscopy from inclusive ψ' and J/ψ radiative decays", Physical Review **D34** (1986) 34.
9. M.A. Shifman, "η_c As We Know It", Z. Phys. **C4** (1980) 345, Erratum-ibid. **C6** (1980) 282.
10. S. J. Brodsky and G. P. Lepage, "Large Angle Two-photon Exclusive Channels in Quantum Chromodynamics", Physical Review **D24** (1981) 1808.
11. S. N. Gupta, J. M. Johnson, and W. W, Repko, "Relativistic two-photon and two-gluon decay rates of heavy quarkonia", Physical Review **D54** (1996) 2075.
12. M. Poppe, "Exclusive Hadron Production in Two-photon Reactions", Int. J. of Mod. Phys. **A1** (1986) 545.
13. V. M. Budnev *et al*, "The Two-photon Particle Production Mechanism. Physical Problems. Applications. Equivalent Photon Approximation", Physics Reports **C15** (1975) 181.
14. T. Feldmann and P. Kroll, "A perturbative approach to the $\eta_c\gamma$ transition form factor", LANL electronic publishing archive hep-ph/9709203, 1997.
15. Y. Kubota *et al*, "The CLEOII detector", Nucl. Inst. and Methods in Physics Research, **A320** (1992) 66.
16. T. Hill, "The CLEOII Silicon Vertex Detector", Nucl. Inst. and Methods in

Physics Research, **A418** (1998) 32.

17. CLEO datasets used a naming convention that had the energy scale the data was taken on (*e.f.* 4s) followed by a number or letter increasing sequentially starting from the first dataset taken on the Υ meson energy. In this naming scheme, we have used the datasets 4s2 through 4sG and 4sJ through 4sT.
18. A. Ershov, "B^0 and B^+ mass measurement", the CLEO collaboration internal note CBX 99-64, 1999.
19. Particle Data Group, "Review of Particle Physics", The European Physics Journal **C** (1998) 141.
20. G. Moneti and X. Xing, "Inclusive Decays $B \to DX$ and $B \to D^*X$", the CLEO collaboration internal note CBX 95-77, 1995.
21. Particle Data Group, "Review of Particle Physics", The European Physics Journal **C** (1998) 146.
22. B. Heltsley, "Luminosity Redux", the CLEO collaboration internal note CBX 93-15, 1993.
23. A. Buijs, "Exclusive Production of Charmonium Resonances at LEP", PHOTON 99 Conference Proceedings, 1999.
24. J. Urheim, "Track-finding Study using Tau-decays", the CLEO collaboration internal note CBX 99-53, 1999.
25. B. Heltsley, "Luminosity Update", the CLEO collaboration internal note CBX 96-40, 1996.
26. R. Galik and E. Kim, "Single Track Trigger Efficiencies in the VD", the CLEO collaboration internal note CBX 00-1, 2000.
27. B. Heltsley, "Update on the Branching Fractions for $\tau \to e\nu\nu_\tau, \mu\nu\nu_\tau$ and $(\pi/K)\nu_\tau$", the CLEO collaboration internal note CBX 96-81, 1996.
28. J. Urheim, "Lepton-Tagged Analysis of $\tau^- \to h^-\pi^0\nu\tau$", the CLEO collaboration internal note CBX 93-127, 1993.
29. D. Acosta, "Investigation into Scintillating Fiber Calorimetry and A Measurement of the Two-Photon Production of Charged Meson Pairs", Ph. D. Thesis, University of California, San Diego, (1993).
30. J. Urheim, "Checking Tails of Resolution", the CLEO collaboration internal note, PhysicsFest 99-6, 1999.
31. D. Bisello *et al*, "Study of the η_c-decays.", Nuclear Physics **B350** (1991) 1.
32. R. M. Baltrusaitis *et al*, "Hadronic Decay of the η_c", Physical Review **D33**

(1986) 629.

33. M. Stancari, "Two Photon Decay Widths of Charmonium Resonances", PHOTON 99 Conference Proceedings, 1999.
34. J. Z. Bai *et al*, "A Measurement of the Mass and Full-Width of the η_c Meson", LANL electronic publishing archive hep-ex/0002006, 2000.
35. T. A. Armstrong *et al*, "Study of the η_c state of charmonium formed in $p\bar{p}$ annihilations and a search for the η_c'", Physical Review **D52** (1995) 4839.
36. C. Baglin *et al*, "Direct Observation and Partial-width Measurement of $\gamma\gamma$ Decay of Charmonium States", Physics Letters **B187** (1987) 191.
37. G. Brandenburg *et al.*, "Measurements of the Mass, Total Width and Two Photon Partial Width of the ETA(C) Meson", Physical Review Letters **85** (200) 3095.
38. R. Brun *et al.*, GEANT 3.15, CERN Report No. DD/EE/84-1, 1987.
39. R. Partridge *et al.*, "Observation of an η_c Candidate State with Mass (2978 $\pm$ 9) MeV", Physical Review Letters **45** (1980) 1150.